

Hyperparameter Transfer with Mixture-of-Experts Layers

Tianze Jiang¹ Blake Bordelon² Cengiz Pehlevan³ Boris Hanin¹

Abstract

Mixture-of-Experts (MoE) layers have emerged as an important tool in scaling up modern neural networks by decoupling total trainable parameters from activated parameters in the forward pass for each token. However, sparse MoEs add complexity to training due to (i) new trainable parameters (router weights) that, like all other parameter groups, require hyperparameter (HP) tuning; (ii) new architecture scale dimensions (number of and size of experts) that must be chosen and potentially taken large. To make HP selection cheap and reliable, we propose a new parameterization for transformer models with MoE layers when scaling model width, depth, number of experts, and expert (hidden) size. Our parameterization is justified by a novel dynamical mean-field theory (DMFT) analysis. When varying different model dimensions trained at a fixed token budget, we find empirically that our parameterization enables reliable HP transfer across models from 51M to over 2B total parameters. We further take HPs identified from sweeping small models on a short token horizon to train larger models on longer horizons and report performant model behaviors.

1. Introduction

Model and data scaling have led to remarkable and often predictable improvements in performance of pretrained deep learning systems (Hestness et al., 2017; Kaplan et al., 2020; Hoffmann et al., 2022; Bergsma et al., 2025b). Realizing in practice the potential benefits conferred by training large models, however, requires carefully tuning hyperparameters (HPs) such as learning rate (schedule), batch size, initialization scale, and weight decay (Li et al., 2025; Wen et al.,

¹Operations Research and Financial Engineering, Princeton University, Princeton, NJ, USA ²Center of Mathematical Sciences and Applications, Harvard University, Cambridge, MA, USA

³John A. Paulson School of Engineering and Applied Sciences, Center for Brain Science, Kempner Institute for the Study of Natural and Artificial Intelligence, Harvard University, Cambridge, MA, USA. Correspondence to: Boris Hanin <bhanin@princeton.edu>.

Preprint. January 29, 2026.

2025). Directly tuning each HP at large scale is typically impractical. As model and data grow, it is therefore crucial to understand how model architecture, optimizer details, and model scale dimensions (e.g. number of layers and hidden width) *jointly* affect training dynamics.

This motivates the study of HP transfer (Yang & Hu, 2022; Yang et al., 2022; Bordelon & Pehlevan, 2022; Bordelon et al., 2023; Yang et al., 2023b; Bordelon & Pehlevan, 2025; Bordelon et al., 2024; Dey et al., 2025; Bergsma et al., 2025a; Wang & Aitchison, 2025), a suite of techniques for obtaining performant HPs in large models directly from good HPs found by tuning substantially smaller models. This HP extrapolation, or transfer, is determined through a *parameterization*, a set of theoretically-motivated rules that predict how variations in each scaling dimension of interest (e.g. model width, depth) should modify raw HP values.

The foundation for the study of HP transfer when scaling width is the so-called max-update parameterization (μ P), first derived for multi-layer perceptrons (MLPs) and validated empirically for more realistic settings in (Yang & Hu, 2022; Yang et al., 2022). Subsequent works (Bordelon et al., 2024; Dey et al., 2025; Bergsma et al., 2025b) provide parameterizations that yield HP transfer for transformer language model pre-training at scale when model width and depth (jointly) grow. The purpose of the present article is to extend such HP transfer techniques to *sparse* Mixture-of-Experts (MoE) models (Shazeer et al., 2017), which replace the dense feedforward (FFN) modules in standard decoder-only transformers (Radford et al., 2019) with layers where only a *fraction* of weights are activated per token, reducing pre-training and inference FLOPS (see Section 3.1 for our exact setup). Our main contributions are as follows:

MoE parameterization. We extend the *CompleteP* parameterization (Dey et al., 2025) (developed for dense transformers) to include MoE-specific scaling rules, allowing for scaling up not only depth and width but also the *number* and *size* of experts (Section 3.3) at fixed active expert sparsity (Section 3.2). Furthermore, we find empirically that training stability in MoEs is more sensitive to *constant-scale* HPs, multipliers that are treated as $\Theta(1)$ in our parameterization (see Apdx. D.1). In contrast, tuning these HPs in dense models can improve performance but does not seem necessary to ensure stability (Bordelon et al., 2023).

Theoretical grounding. We provide a theoretical justification of our proposed parameterization using dynamical mean-field theory (DMFT) (Bordelon & Pehlevan, 2022). Specifically, we obtain an explicit description of the training dynamics of residual networks with MoE layers in the *simultaneous* limit of infinite width, depth, expert size, and expert count. The evolution of (finite) network summary statistics (e.g. layerwise feature kernels) is therefore automatically consistent across scale. We find a novel three-level mean-field hierarchy: residual stream representations are mean-field over expert outputs, which are themselves mean-field over individual expert neurons. The DMFT analysis justifies several subtle but important properties of our parameterization, such as the transfer of optimal HPs across expert hidden width multiplier (Figure 2, last column).

Empirical validation of HP transfer. We systematically verify (over different datasets and MoE sparsity levels) that our parameterization enables reliable transfer on both the initialization scale (init. std. σ) and learning rate (LR η) when varying width, depth, expert count, and expert size (Figure 2 and Figure 4) on a fixed token budget (1B). We verify HP transfer by tuning base models with 38M activated parameters and scale up to (around) 2B total parameters (Figure 2 and Figure 13).

Performant models. We find empirically that using our parameterization to select HPs leads to strong pre-training performance, even when compared to competitive dense baselines (Figure 1 and Figure 15) when scaling up both model dimensions and increasing total training steps (and thus total number of tokens). Furthermore, our parameterization consistently exhibits uniform expert load balancing even when expert count is scaled (Figure 17).

Insights on architecture shapes. We empirically verify, via our zero-shot optimal HP, existing findings (Krajewski et al., 2024; Boix-Adsera & Rigollet, 2025) on scaling expert size versus expert count in MoEs. Without the need to retune HPs at each scale, we consistently recover the benefit of increasing number of experts over expert sizes at fixed parameter count (Figure 5 and Figure 16).

2. Related backgrounds

Mixture of Experts. Mixture of Experts (MoE) layers represent a paradigm shift in neural architecture design, decoupling parameter count from computational cost via conditional routing, and significantly reducing FLOP at both training and inference. Modern implementations of these architectures, pioneered by (Shazeer et al., 2017) and scaled through GShard (Lepikhin et al., 2020) and Switch Transformer (Fedus et al., 2022), utilize a learned gating mechanism to route tokens to a sparse subset of top-k experts as a way to deploy models with trillions of parameters while

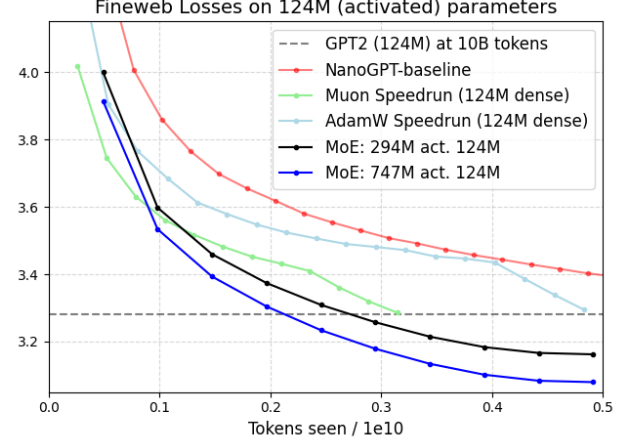


Figure 1. Matching active architecture to be GPT2-small (124M) and 500K batch size, comparison of MoE training loss on our zero-shot Adam HPs (found from tuning 38M activated base models) on FineWeb versus (dense GPT) baseline (Karpinsky, 2023), speedrun AdamW, and speedrun Muon loss curves (Jordan & contributors, 2025) towards the 3.28 val. loss for baseline at 10B tokens. See Section 5 for details. Dense benchmarks are taken before Oct.14, 24, with advanced mods such as zero down-proj. and QK-norms.

maintaining per-token computation of much smaller dense models. Recent progress such as Mixtral 8x7B (Jiang et al., 2024), Expert-Choice (Zhou et al., 2022), the DeepSeek-MoEs (Liu et al., 2024; Dai et al., 2024) have further refined architectural details such as routing strategies (e.g., shared experts, loss-free load balancing) to maximize knowledge specialization and training efficiency. However, despite these advances, language model pretraining at scale remains difficult due to challenges such as expert collapse (where the router favors only a few experts), dead or super experts (Su et al., 2025), and training instability (Zoph et al., 2022), often requiring complex ad-hoc strategies to overcome.

HP transfer and DMFT. Traditional approaches to HP tuning at large scale require either grid-searching in a large model or extrapolating from power laws fit to a family of smaller models (Li et al., 2025; Zhou et al., 2026). Instead, our approach seeks the direct (rule-based) transfer of optimal HP from small models to larger ones. The core behind transfer is parameterizations that stabilize the forward and backward passes across scales. First studied for scaling the width of MLPs, this stability condition resulted in two types of parameterizations: the *Neural Tangent* parameterization (NTP) (Hayou et al., 2022; Jacot et al., 2020; Roberts et al., 2022) and the *Mean-Field* parameterization (MFP) (Mei et al., 2018; Chizat et al., 2019; Rotskoff & Vanden-Eijnden, 2022). Such stability conditions have also been studied via the modular norm (Large et al., 2024) and effective field theory (Dinan et al., 2023; Yaida, 2022; Roberts et al., 2022).

The seminal works (Yang & Hu, 2022; Yang et al., 2023a) introduce the concept of a max-update parameterization (μ P), defined by a set of explicit feature learning desiderata

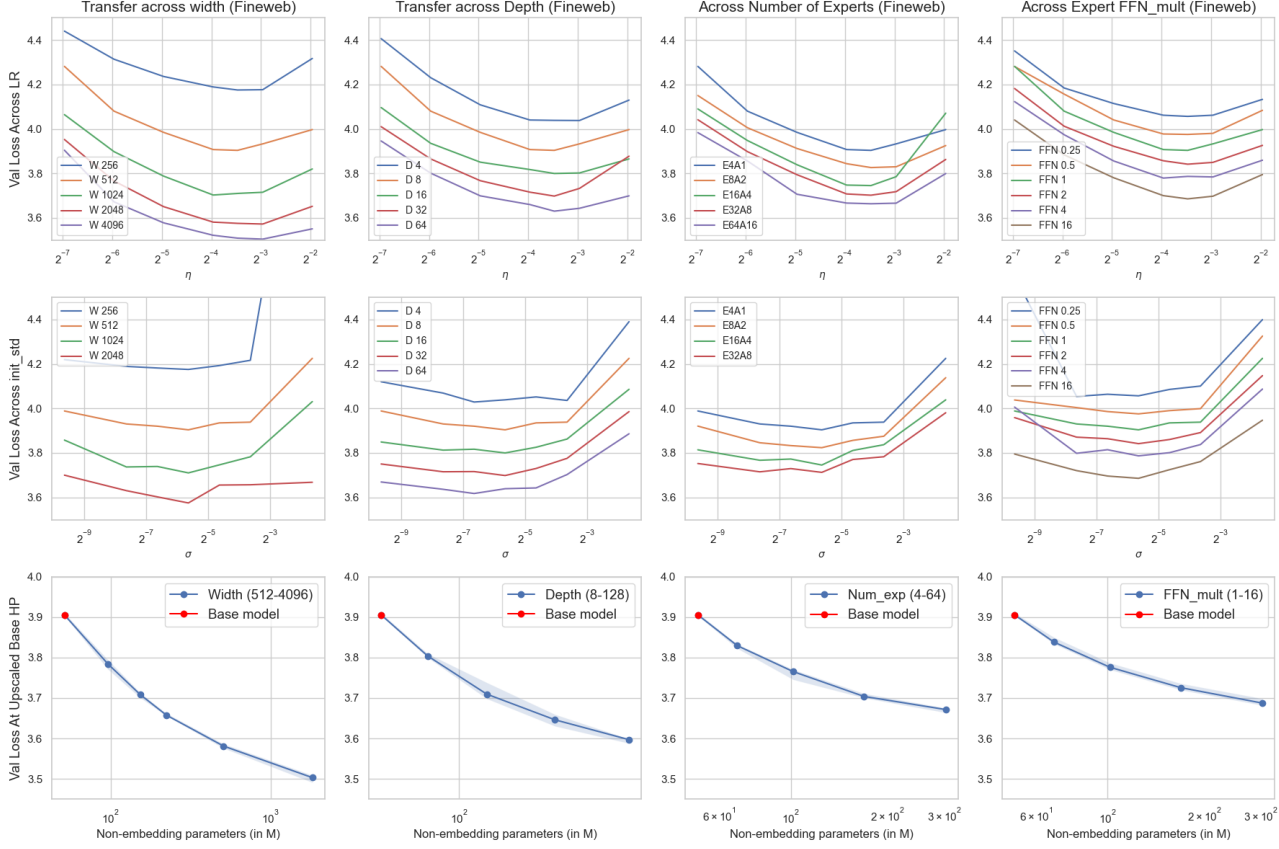


Figure 2. Global base learning rate (first row) and global base init (second row) transfer trained on 1B tokens (2000 steps) on the Fineweb dataset, with different model sizes from 20M to 1.8B scaling across width, depth, number of experts (fixing sparsity), and expert MLP hidden multiplier. We fix the base config ($n_{\text{emb}} (W) = 512$, $L = 8$, $(n_{\text{exp}}, n_{\text{act}}) = (4, 1)$ ('E4A1' in the figure), $\alpha = 1$) and vary one dimension at a time. Error bars in the last row are (max, min, and median) over four independent seeds. See Section 5 for details.

satisfied by MFPs and empirically enabling direct *transfer* of good hyperparameters. More recent works (Dey et al., 2025; Mlodzeniec et al., 2025) extended μ P to allow for depth, width, and other scale parameters in practical-sized (dense) LLM pretraining on compute-optimal horizons.

Dynamical mean-field theory (DMFT) provides a way to theoretically analyze HP transfer by showing which parameterizations cause training dynamics of finite networks to converge to a well-defined limit. This framework traces the evolution (in infinite-sized networks) of mean-field model statistics, such as inner-product kernels for hidden activations and gradients. DMFT results were first derived for MLPs (Bordelon & Pehlevan, 2022) and later extended for multi-head self-attention (Bordelon et al., 2024), transformers in the infinite-depth limit (Bordelon et al., 2023), and finite-width correction (Bordelon & Pehlevan, 2025). We refer to Sec.4 in (Bordelon et al., 2023) for a more thorough explanation of how DMFT backs up HP transfer.

Concurrent work. Independent and concurrent work (Malasnicki et al., 2025) also studies LR transfer in MoE models as the embedding width scales. However, our contrib-

utions go beyond in several ways: (1) We study transfer of not only base LR but also init. scale, on not only width but also on depth, number of experts, and experts sizes, while reporting a full suite of auxiliary empirical details, and (2) we back our parameterization with novel DMFT analysis (Section 4) that goes beyond calculating μ P gradient heuristics, demonstrating novel theoretical insights.

3. Scaling recipe for MoEs models

We begin by detailing in Section 3.1 the MoE transformer architecture used in our experiments. We then briefly justify in Section 3.2 why we fix expert sparsity across increasing model size. Finally, in Section 3.3 we adapt from μ P (Yang & Hu, 2022) and CompleteP (Dey et al., 2025) to provide a heuristic derivation of our proposed parameterization.

3.1. Model setup

Our theory and experiments concern decoder-only Transformer language models (Radford et al., 2019) with MoE modules in the feed-forward (FFN) layers. In this architec-

ture, a sequence of T input tokens is mapped to an output by first up-projecting (along with positional embedding) each token to a sequence $h^{(0)}$ in $\mathbb{R}^{n_{\text{embd}} \times T}$. This initializes the residual stream, whose updates are computed through $2L$ residual layers that intersperse L pre-LayerNorm multi-head self-attention (MHSA) blocks (for $\ell = 1, \dots, L$):

$$h^{(2\ell+1)}[0:T] = h^{(2\ell)}[0:T] + \frac{1}{L} f_{\text{MHSA}}(\text{LN}(h^{(2\ell)}[0:T]))$$

with L pre-LayerNorm MoE layers (applied position-wise)

$$h^{(2\ell+2)} = h^{(2\ell+1)} + \frac{1}{L} f_{\text{MoE}}(\text{LN}(h^{(2\ell+1)})).$$

An un-embedding layer down-projects the final residual representation $h^{(2L)}$ to produce an output. The $1/L$ multipliers on residual block outputs are chosen following results in (Dey et al., 2025), which give a parameterization called *CompleteP* that ensures HP transfer when scaling depth and embedding dimension in dense models. Our parameterization keeps *CompleteP* unchanged when scaling depth and width but allows for separately scaling both expert width and number of experts in the MoE module

$$f_{\text{MoE}}(h) \triangleq \frac{1}{n_{\text{act}}} \sum_{i \in A(h)} g_i(h) \cdot E_i(h) \in \mathbb{R}^{n_{\text{embd}}}, \quad (1)$$

where $g_i(h) \triangleq \sigma(r_i) \in \mathbb{R}$ are (un-normalized) mixing coefficients, σ is a non-linear activation function, and

$$r_i \triangleq \left(W_{\text{router}}^{(i)} \right)^T h \in \mathbb{R}, \quad W_{\text{router}}^{(i)} \in \mathbb{R}^{n_{\text{embd}}}.$$

The activated set $A(h) \subseteq \{1, \dots, n_{\text{exp}}\}$ is a token-dependent subset with n_{act} indices of *activated experts* determined by

$$A(h) = \text{top}_{n_{\text{act}}}(\{g_i(h) + b_i; i = 1, 2, \dots, n_{\text{exp}}\})$$

in which expert biases $b_i \in \mathbb{R}, i = 1, \dots, n_{\text{exp}}$ are trainable and *only* participate in the hard-routing. We take each expert E_i to be a single hidden-layer MLP

$$E_i(h) = W_{\text{down}}^{(i)} \phi \left((W_{\text{up}}^{(i)})^T h \right) \in \mathbb{R}^{n_{\text{embd}}}$$

with a hidden layer of size $\alpha_{\text{ffn}} \cdot n_{\text{embd}} \in \Omega(n_{\text{embd}})$, and $W_{\text{up}}^{(i)}, W_{\text{down}}^{(i)} \in \mathbb{R}^{n_{\text{embd}} \times \alpha_{\text{ffn}} n_{\text{embd}}}$. To be close to our theoretical analysis (Section 4), our setup disentangles inter-expert router weights (following (Wang et al., 2024)): for each expert i , router $g_i(h)$ *only* depends on $W_{\text{router}}^{(i)} \in \mathbb{R}^{n_{\text{embd}}}$. Practically, we did not observe significant differences in model performance across scale between different types of mixing coefficients (e.g., topK-then-softmax, softmax-then-topK).

Training. We consider the standard Adam optimizer (Kingma & Ba, 2017) (see Apdx. C for discussion on weight

Parameter	Dimension	Init Std	LR
Router	$\mathbb{R}^{n_{\text{embd}} \times n_{\text{exp}}}$	$n_{\text{embd}}^{-\gamma}$	n_{embd}^{-1}
Expert bias	$\mathbb{R}^{n_{\text{exp}}}$	0	1
Expert (up)	$\mathbb{R}^{n_{\text{embd}} \times \alpha_{\text{ffn}} n_{\text{embd}}}$	$n_{\text{embd}}^{-1/2}$	n_{embd}^{-1}
Expert (dn)	$\mathbb{R}^{n_{\text{embd}} \times \alpha_{\text{ffn}} n_{\text{embd}}}$	$n_{\text{embd}}^{-1/2} \alpha_{\text{ffn}}^{-1}$	$n_{\text{embd}}^{-1} \alpha_{\text{ffn}}^{-1}$

Table 1. Parameter groups and their scaling rules for the MoE module at each layer as per derivation in Section 3.3.

decay). During training, we treat the activated experts sets $A(h)$ in each layer as no-grad vectors, and router matrices *only* receive gradients through the expert mixing coefficients $g_i(h)$. Writing $\text{Load}_i \in [0, 1]$ for the (batch) proportion of tokens routed to expert E_i , we encourage *expert load-balancing*, i.e. we ask that

$$\text{Load}_i \approx \kappa \triangleq n_{\text{act}}/n_{\text{exp}},$$

ensuring that the fraction of tokens routed to each expert is approximately the same. In contrast to a line of prior works (Shazeer et al., 2017; Fedus et al., 2022) which uses an auxiliary loss as regularization to balance expert load, we adapt the auxiliary-loss-free (Wang et al., 2024; Liu et al., 2024) framework, which encourages expert load balancing by (only) directly updating expert biases

$$b_i \leftarrow b_i - \eta_{\text{bias}} \cdot (\text{Load}_i - \kappa) \quad (2)$$

without affecting updates to other weights. See Apdx. D.2 for further discussion around this choice.

3.2. Scaling that preserves sparsity versus topK

Let us briefly explain and emphasize an important design choice for scaling: we scale up $n_{\text{exp}}, n_{\text{act}} \rightarrow \infty$ while preserving sparsity $\kappa = n_{\text{act}}/n_{\text{exp}}$ (which we think of as a small positive constant). This is instead of scaling up n_{exp} while fixing n_{act} (Fedus et al., 2022) and sending $\kappa \rightarrow 0$.

We have three practical motivations for this choice. First, (assuming perfect balancing) in a batch of B tokens, each MoE expert sees only κB tokens, whereas attention and routing modules see the full B tokens. This suggests HPs will not transfer across different κ (this is partly confirmed in Figure 10). Second, for large deployments, it has been empirically reported that the range of optimal sparsity κ is often hardware-controlled (StepFun et al., 2025) and bounded below. Finally, a constant κ is natural in the mean-field analysis (Sec. 4) as it represents conditioning on a constant-probability event when integrating over the mean-field measure of experts. Our theory suggests that HPs will transfer at fixed κ and our empirical results support this point.

3.3. MoE Parametrization

For each parameter group (e.g. routing weights, up/down projections in each expert, and expert biases), a practitioner

must specify two hyperparameters: initialization std. and learning rate. By a parameterization, we mean a set of rules for how, given a set of HPs for a model at one scale to construct a corresponding set of HPs after up-scaling some of the model dimensions depth L , width n_{embd} , expert width (governed by $\alpha_{\text{ffn}} \in \Omega(1)$), and expert count n_{exp} .

Prior work, notably (Yang et al., 2022; Bordelon et al., 2024; Dey et al., 2025), derived parameterizations for dense transformers that exhibit HP transfer across model width and depth. We adopt those prescriptions and focus here on adapting them for sparse MoEs scaling n_{embd} and n_{exp} at fixed sparsity κ . That is, we describe how to set initialization variances and Adam learning rates for router weights $W_{\text{router}}^{(i)}$, MLP expert down/up projections $W_{\text{down/up}}^{(i)}$ and expert biases b_i . Our derivations follow ideas introduced in the max-update (μP) (Yang & Hu, 2022) and later refined in (Bordelon et al., 2024; Dey et al., 2025). Our results (proposed parameterization) are summarized in Table 1.

Notation. For any vector $\theta \in \mathbb{R}^k$ we will shorthand $\theta \in \Theta(C)$ to denote $\|\theta\|_2^2 \in \Theta(k \cdot C)$. To derive scaling rules for Adam, we will also use $\overline{\nabla W}$ to denote the normalized Adam update per step $W_{t+1} \leftarrow W_t - \eta \overline{\nabla W}_t$ and use Adam’s approximation to SignGD ($\overline{\nabla W} \in \{-1, 1\}^*$) (Bernstein et al., 2018) so $\Delta w = \eta \overline{\nabla w} \approx \eta \cdot \text{sgn}(\frac{\partial w}{\partial \Theta})$ for any weight group w . We also use $\cos(v_1, v_2) = v_1^T v_2 / \|v_1\|_2 \|v_2\|_2$ to denote the cosine of angle between two vectors.

Operationalizing μP and CompleteP . A core tenant of the μP (Yang & Hu, 2022) and CompleteP (Dey et al., 2025) approach to HP transfer is to choose init. and LR so that components of network pre-activations and residual blocks are $\mathcal{O}(1)$ at init. and are updated by $\Theta(1)$ after every step of training. To operationalize this for Mixture-of-Experts, we require a stronger condition where max-update conditions have to also hold for *each* individual expert component (mixing coefficient and expert output). We denote schematically by z either the MoE layer output f_{MoE} , individual expert output $E_i(h)$, mixing coefficient $g_i(h)$, or an expert hidden layer representation $h_{\text{up}}^{(i)} \triangleq (W_{\text{up}}^{(i)})^T h \in \mathbb{R}^{\alpha_{\text{ffn}} n_{\text{embd}}}$ for $i = 1, 2, \dots, n_{\text{exp}}$. Viewing these as functions of the MoE parameters W , our heuristic requires that the change in z from the corresponding W separately:

$$\eta_W \overline{\nabla W} \frac{\partial z}{\partial W} = \Delta W \frac{\partial z}{\partial W} = \Theta(1). \quad (3)$$

Router weights. We start with deriving the parameterization for the MoE router matrix W_{router} . We apply (3) on $W = W_{\text{router}}^{(i)}$ and $z = g_i(h) = \sigma(h^T \cdot W_{\text{router}}^{(i)})$. Assuming that $\sigma'(\cdot) \in \Theta(1)$, we arrive at our first desiderata:

Desideratum 1. *We want for each $i = 1, \dots, n_{\text{exp}}$ that*

$$h^T \cdot \Delta W_{\text{router}}^{(i)} = \Theta(1).$$

where $h \in \Theta(1)$ from pre-LayerNorm.

Recall $\Delta W_{\text{router}}^{(i)} = -\eta_{\text{router}} \overline{\nabla W}_{\text{router}}^{(i)}$. We assume

$$\frac{h^T \cdot \overline{\nabla W}_{\text{router}}^{(i)}}{\|\overline{\nabla W}_{\text{router}}^{(i)}\|_2 \|h\|_2} = \cos\left(\overline{\nabla W}_{\text{router}}^{(i)}, h\right) \in \Theta(1),$$

referred to as the “Law of Large Numbers” type of alignment between vectors in (Yang & Hu, 2022). Since $\|\Delta W_{\text{router}}^{(i)}\|, \|h\| \in \Theta(\sqrt{n_{\text{embd}}})$, the above leads to

Scaling Rule 1. *The router matrix $W_{\text{router}}^{[n_{\text{exp}}]}$ has learning rate $\eta_{W_{\text{router}}^{[n_{\text{exp}}]}} \in \Theta(1/n_{\text{embd}})$.*

At initialization, $z = g_i \in \mathcal{O}(1)$ requires $W_{\text{router}}^{(i)} \in \Theta(n_{\text{embd}}^{-\gamma})$ for $\gamma \geq 0.5$ (again, when $\Delta z \in \Theta(1)$, it is not necessary to initialize at $\Theta(1)$). Empirically, we observed no practical impact of the router initialization scaling on the loss, so long as it is not numerically too large. In the literature, (Shazeer et al., 2017) used $\gamma = \infty$ (zero router initialization) to ensure load balancing at step 0, (Lepikhin et al., 2020) used $\gamma = 1/2$ such that router logits are $\Theta(1)$ at init, and (Malasnicki et al., 2025) argues for $\gamma = 1$, which mimics the final layer of mean-field MLPs. All experiments are done with $\gamma = 1$ in the main text.

Expert biases. For expert biases, we only need to track how much each update shifts the activated experts set. While $b_{[n_{\text{exp}}]}$ only participate in hard-routing, the spirit of (3) can be carried via tracking f_{MoE} update by updating b alone:

$$\Delta_b f = \frac{1}{n_{\text{act}}} \left[\sum_{A_{t+1}(h) \setminus A_t(h)} g_i E_i - \sum_{A_t(h) \setminus A_{t+1}(h)} g_i E_i \right]$$

which leads to (assuming $g_i, E_i \in \Theta(1)$):

Desideratum 2. *For each step of update on $b_{[n_{\text{exp}}]}$, the activated set of expert shifts by at least $|A_t(h) \setminus A_{t+1}(h)| \in \Theta(n_{\text{act}})$ (for fixed W_{router}).*

We defer the derivation of η_{bias} to Apdx. B. As before, max-update principles place no requirement on initialization so long as $b \in \Theta(1)$. However, taking into account expert load balancing, we conveniently initialize biases at zero so no one expert receives dominant tokens (or no tokens) at init.

Scaling Rule 2. *Expert biases $b_{[n_{\text{exp}}]}$ are initialized at zero with LR $\eta_{\text{bias}} \in \Theta(1)$.*

Experts MLP weights. This part largely follows from the standard μP derivations except for the added dimension in α_{ffn} , which was covered in the heuristics of (Yang et al., 2023a) and rigorously studied in (Chizat, 2025) in the finite n_{embd} and large L limit. A heuristical justification is to imagine $n_{\text{embd}} = 1$ then take α_{ffn} as the intermediate “width” in a two-layer MLP under the mean-field

parametrization (and thus different from the typical ‘‘fan-in’’ initialization, which resembles the NTP concerning α_{ffn} , see Figure 11 for a simple ablation). For each individual expert, dropping expert indices, recall again:

$$h_{\text{up}} \triangleq (W_{\text{up}})^T h \in \mathbb{R}^{\alpha_{\text{ffn}} n_{\text{embd}}}; E(h) = W_{\text{down}} \phi(h_{\text{up}})$$

where $W_{\text{up}}, W_{\text{down}} \in \mathbb{R}^{n_{\text{embd}} \times \alpha_{\text{ffn}} n_{\text{embd}}}$. Our goal from (3) is to force $\Delta h_{\text{up}}, \Delta E \in \Theta(1)$ from each step of training by updating individual weight components. Note that

$$\begin{aligned} \Delta h_{\text{up}} &= (W_{\text{up}})^T \Delta h + \Delta (W_{\text{up}})^T h \\ \Delta E &= W_{\text{down}} \Delta \phi(h_{\text{up}}) + \Delta W_{\text{down}} \cdot \phi(h_{\text{up}}) \\ &= W_{\text{down}} \text{diag}(\phi'(h_{\text{up}})) \Delta h_{\text{up}} + \Delta W_{\text{down}} \cdot \phi(h_{\text{up}}) \end{aligned}$$

Assuming that $\phi'(\cdot) \in \Theta(1)$, our conditions are:

Desideratum 3. *During each step of training update,*

$$(W_{\text{up}})^T \Delta h, h^T \Delta W_{\text{up}}, W_{\text{down}} \Delta h_{\text{up}}, \Delta W_{\text{down}} \phi(h_{\text{up}})$$

are all in $\Theta(1)$.

Assume for all individual neurons $j \in [\alpha_{\text{ffn}} n_{\text{embd}}]$:

$$\frac{h^T (\Delta W_{\text{up}})_j}{\|\Delta (W_{\text{up}})_j\|_2 \|h\|_2} = \cos(\Delta (W_{\text{up}})_j^T, h) = \Theta(1)$$

which dictates LR for the up-projection via requiring that $\|\Delta (W_{\text{up}})_j\|_2 \in \Theta(\|h\|_2^{-1}) = \Theta(n_{\text{embd}}^{-1/2})$. For σ_{init} ,

$$\Theta(\sqrt{\alpha_{\text{ffn}} n_{\text{embd}}}) \ni \|(W_{\text{up}})^T \Delta h\|_2 \approx \|\Delta h\|_2 \|W_{\text{up}}\|_{\text{op}}$$

and given that $\|\Delta h\|_2 \approx \sqrt{n_{\text{embd}}}$ we get $\|W_{\text{up}}\|_{\text{op}} \in \Theta(\sqrt{\alpha_{\text{ffn}}})$. We can thus conclude following standard results from random matrix theory $\|W_{\text{up}}\|_{\text{op}} \approx \sqrt{\alpha_{\text{ffn}} n_{\text{embd}}} \sigma_{\text{init}}$ when assuming $\alpha_{\text{ffn}} \in \Omega(1)$.

For the down-projection layers, similar derivations can be made for the learning rate, where we assume that the up-projected embedding is correlated with weight updates $\cos(\Delta (W_{\text{down}}), \phi(h_{\text{up}})) = \Theta(1)$ across all neurons. For the initialization scale, our conditions require the following norm to be in $\Theta(n_{\text{embd}}^{1/2})$:

$$\begin{aligned} \|W_{\text{down}} \Delta h_{\text{up}}\|_2 &\approx \|\Delta h_{\text{up}}\|_2 \|W_{\text{down}}\|_{\text{op}} \\ &\approx \sqrt{\alpha_{\text{ffn}} n_{\text{embd}}} \sqrt{\alpha_{\text{ffn}} n_{\text{embd}}} \sigma_{\text{init}} (W_{\text{down}}) \end{aligned}$$

when $\alpha_{\text{ffn}} \in \Omega(1)$. Combined with the above, we have:

Scaling Rule 3. *For the MLP Experts, we have*

$$\sigma_{\text{init}}(W_{\text{up}}^{(i)}) = n_{\text{embd}}^{-1/2}, \quad \eta(W_{\text{up}}^{(i)}) = n_{\text{embd}}^{-1}$$

and

$$\sigma_{\text{init}}(W_{\text{down}}^{(i)}) = \alpha_{\text{ffn}}^{-1} n_{\text{embd}}^{-1/2}, \quad \eta(W_{\text{down}}^{(i)}) = \alpha_{\text{ffn}}^{-1} n_{\text{embd}}^{-1}$$

for all $i \in \{1, 2, \dots, n_{\text{exp}}\}$.

4. Dynamical mean field theory

To theoretically establish that our parameterization enables a scale-invariant well-defined limit (and consequently admits HP transfer across jointly scaling model dimensions), we study the training dynamics for a deep residual MoE model with diverging residual stream width and expert count $n_{\text{embd}}, n_{\text{exp}} \rightarrow \infty$ with activated experts $n_{\text{act}} = \kappa n_{\text{exp}}$. We can also optionally take the expert size $n_{\text{hid}} \triangleq \alpha_{\text{ffn}} n_{\text{embd}} \rightarrow \infty$ and the depth $L \rightarrow \infty$ so long as $n_{\text{embd}}/(n_{\text{exp}} n_{\text{hid}} L)$ is bounded in the limit. We find that the MoE dynamics have a three-level mean-field structure¹:

1. The network outputs are determined by population averages over residual stream neurons and averages over the state of the experts within each hidden MoE layer. Residual stream neurons are mean-field in the $n_{\text{embd}}, n_{\text{exp}} \rightarrow \infty$ limit. The macroscopic behavior of the network is summarized by averages (denoted by $\langle \cdot \rangle$) over the residual stream neuron distribution.
2. Each expert is characterized by a collection of scalar variables that include the router pre-activation and bias. These expert state variables are mean-field in the $n_{\text{embd}}, n_{\text{exp}} \rightarrow \infty$ limit, with averaging denoted as $[\cdot]$. The top- n_{act} action is determined by expert random variables $q = \sigma(r) + b$ and hard gating is set by a quantile threshold $q_{\star}(\kappa)$ which satisfies $[\mathbf{1}_{q \geq q_{\star}(\kappa)}] = \kappa$. The (hard) gating variables for each expert are thus $\sigma \triangleq \mathbf{1}_{q \geq q_{\star}(\kappa)} \sigma(r)$.
3. Within each expert, hidden neuron states are mean-field in the $n_{\text{hid}} \rightarrow \infty$ limit. Their dynamics depend on all three levels of the mean-field hierarchy. We denote averaging over the within-expert neurons $\{\cdot\}$.

At a high level, the training dynamics close in terms of a finite set of deterministic quantities \mathbf{Q} which include correlation and response kernels, as well as the network output. Some examples of the relevant correlation kernels include

$$\begin{aligned} C_h^{\ell}(x, x', t, t') &= \langle h^{\ell}(x, t) h^{\ell}(x', t') \rangle \\ M_{\sigma \sigma C_{\phi_k}}^{\ell}(x, x', t, t') &= [\sigma^{\ell}(x, t) \sigma^{\ell}(x', t') \{ \phi(h^{\ell}(x, t)) \phi(h^{\ell}(x', t')) \}] . \end{aligned} \quad (4)$$

for input x at time t . We derive the full set of closed evolution equations for the macroscopic variables \mathbf{Q} that govern the network outputs in Appendix E. Some useful observations can be immediately gleaned from the theory:

1. If $n_{\text{embd}}, n_{\text{exp}}, n_{\text{hid}} \rightarrow \infty$ with $\alpha_{\text{ffn}} \in \Theta(1)$, the resulting dynamics are independent of the FFN ratio α_{ffn} .

¹By saying ‘‘ X is mean-field’’, we mean the dynamics of each individual element of the population depend only on itself and averages over the entire population. See Apdx E for details.

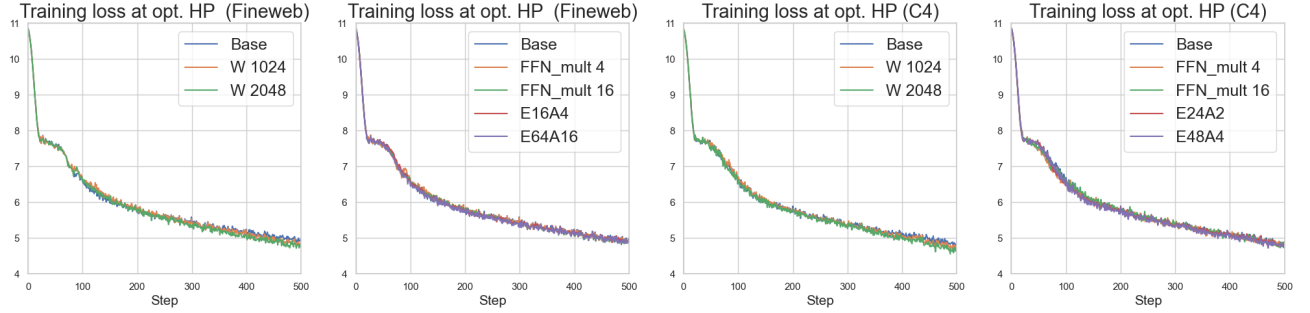


Figure 3. (Finding 1.2): Loss curve collapse (scale invariance) of model scaling dimension (in earlier steps) when scaling up the base model in different ways. Parts (1) and (2): Fineweb dataset on sparsity 1/4. Parts (3) and (4): C4 dataset on sparsity 1/12.

This is similar to findings at large depth in dense models (Chizat, 2025) and provides a theoretical basis for transfer across α_{ffn} as in Figure 2.

2. n_{hid} does not need to diverge for network outputs and residual stream measures to concentrate. If $n_{\text{embd}}, n_{\text{exp}} \rightarrow \infty$ with $n_{\text{exp}}/n_{\text{embd}} = \nu$, the output of the network obeys a deterministic evolution which depends on n_{hid} explicitly, but not on ν , similar to dependence on head size in mean-field limits of attention blocks (Hron et al., 2020; Bordelon et al., 2024). This MoE regime is empirically studied in (He, 2024).
3. A large family of joint scalings generates identical dynamics. Let $n_{\text{embd}}(N), n_{\text{hid}}(N), n_{\text{exp}}(N), L(N)$ be diverging functions. The limiting dynamics are universal if $\alpha_* \triangleq \lim_{N \rightarrow \infty} \frac{n_{\text{embd}}(N)}{n_{\text{hid}}(N)n_{\text{exp}}(N)L(N)} = 0$.
4. The depth limit $L \rightarrow \infty$ generates a neural ODE for each hidden neuron on the residual stream if $\alpha_* = 0$ (Bordelon et al., 2024; Dey et al., 2025; Chizat, 2025), but can generate a neural SDE if $\alpha_* > 0$ (Bordelon et al., 2023; Yang et al., 2023b).

A similar three-level structure also appears in multi-head self-attention, where there is a measure over attention heads (analogous to the expert measure) and an additional measure of key-query neurons within each head (Bordelon et al., 2024). Combining our novel analysis of the MoE layers with the existing DMFT for multi-head attention yields a complete description of sparse transformers in this work. Further details are deferred to Appendix E.

5. Empirical results and findings

Our experiments focus on MoE architectures described in Section 3.1, and we defer training details to Appendix A.

We consider two different expert activation sparsity on two different natural language datasets: (i) Sparsity $\kappa = 1/4$, on the FineWeb dataset (Penedo et al., 2024); and (ii) Sparsity $\kappa = 1/12$, on the C4 (Colossal Clean Crawled Corpus) dataset (Raffel et al., 2020).

In all of our experiments under a fixed token budget, we use a total of (roughly) 1B tokens divided into 2000 batches of 500K tokens and context length 1024. We use an LR scheduler with a linear warmup phase for the first 1000 steps and stable (constant) LR for the latter half. While a typical LR schedule does not warm up for half of the training iterations, our goal with the fixed token budget experiments is to model an early checkpoint or a larger run, which often contains 0.5B (or more) tokens during the warm-up phase.

For each parameter group, we also tune constant-scale multipliers on the learning rate and initialization. Without tuning constant multipliers, we found that (1) nontrivial performance was left on the table and (2) training dynamics (e.g. load balancing loss) can become unstable even at around the optimal HP. See Appendix D.1 for details

5.1. Experiment findings for fixed token budget

Finding 1.1. Fixing the sparsity ratio and token budget, optimal base LR and initialization standard deviation transfer across different dimensions of model scale.

Figure 2 and Figure 4 show the main results in this paper: under our scaling rules, relevant hyperparameters are transferred across multiple model dimensions. Furthermore, we also find that the optimal HP identified from small models enables uniform expert load across all experts (Figure 17).

Finding 1.2. On the upscaled optimal HPs, loss profiles in early iterations collapse to that of the base model as width, number of experts, and expert sizes increase.

As supporting evidence to Section 4, we demonstrated (Figure 3) that, in our class of scaling models, the training loss profile in early iterations collapses entirely before diverging (where larger models have lower losses). The finding also echoes known results on dense models, albeit for longer training horizons (Bergsma et al., 2025b; Qiu et al., 2025).

5.2. Experiments on larger token-horizon

We scale up HPs found from 38M active base model on 1B tokens to longer training horizons under the same batch-size

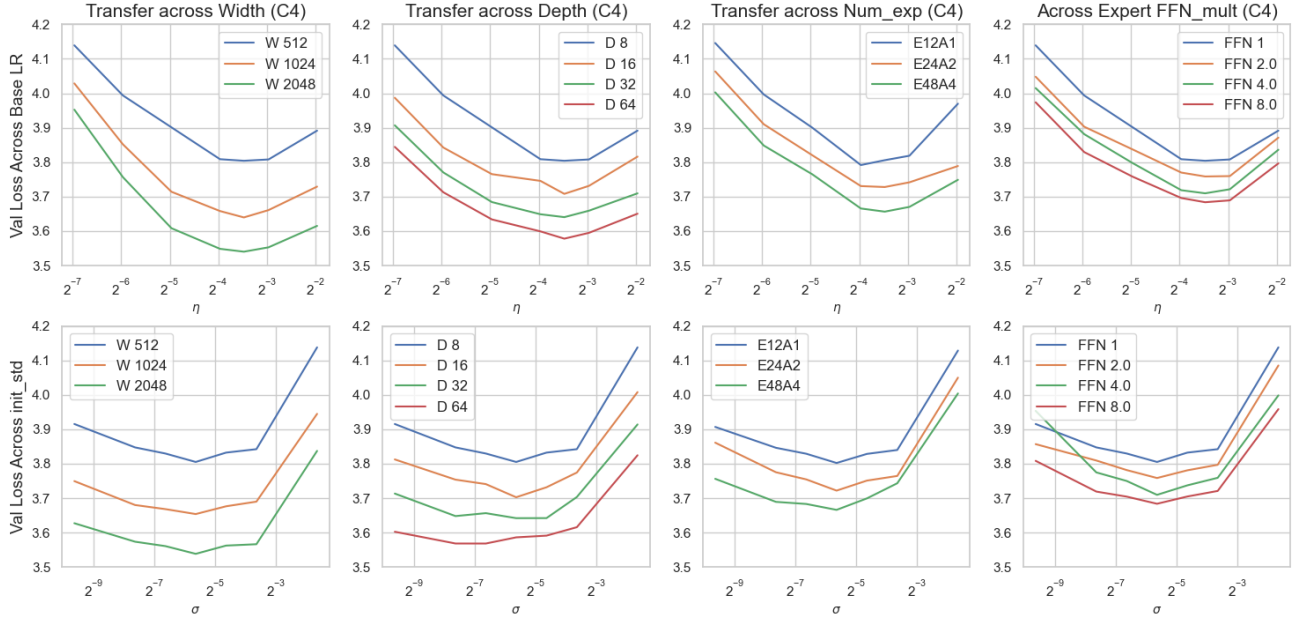


Figure 4. Fixed token transfer of global base LR (row 1) and global base init (row 2) on $\kappa = 1/12$ and the C4 dataset

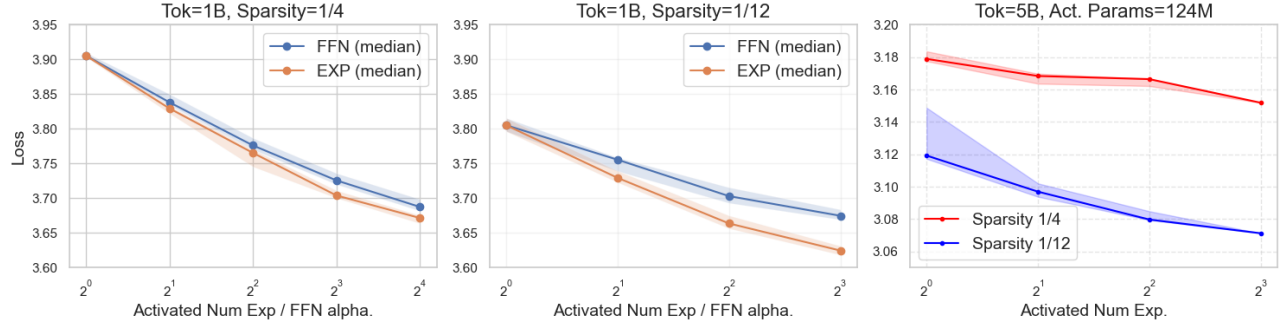


Figure 5. Parts (1) and (2): At a fixed token budget of 1B, scaling up from the base model (1 activated expert and expert $\alpha_{\text{ffn}} = 1$), increasing the number of experts is more parameter-efficient than expert size. Error bars are (min, median, max) out of 4 seeds. Part (3): At a 5B token horizon with GPT2-small activated and cosine LR cool-down to zero, having more activated experts (and thus smaller experts) monotonically improves performance. Error bars for $n_{\text{act}} \leq 4$ are (min, median, max) out of 3 seeds.

and more steps (while keeping the 0.5B token warmup fixed). Fixing the activated architecture per token (which resembles a standard dense transformer), we can also compare our MoE (with up-scaled HP) training versus known results in dense models (matching active parameter count).

Finding 2.1. The optimal HPs found from small models enable stable training on longer total token horizons and achieve competitive loss (against active parameter-matched dense models).

Fixing the architecture of the total activated model to match that of the Nano-GPT implementation of GPT2-small (124M) (and having more total parameters), we report a competitive loss curve via zero-shot HPs (Figure 1) compared to checkpoints of the (dense) GPT2-Fineweb speedrun (Jordan & contributors, 2025) under the same batch size. See also Figure 15 for running 7.5B tokens on GPT2-medium (355M activated). For training with a large number of steps, while

fixing a stable LR after warmup still yields stable and converging training, including a LR decay (even the simplest cosine decay to zero) empirically improves final validation performance in our experiments.

5.3. Tradeoff between expert count versus expert size

We can now study architectural properties such as the trade-off between expert count and expert size while fixing sparsity and number of parameters.

Finding 3.1. An increasing number of experts while fixing the total parameter improves the final model performance.

We justify it via Figure 5 and in Apdx D.3 for smaller models trained on a longer token horizon. While previous works reported benefits of more smaller experts (Krajewski et al., 2024; Liu et al., 2024; Boix-Adsera & Rigollet, 2025), our HP transfer enables such a comparison to be fair and cheap.

6. Conclusion and future directions

In this work, we derived a novel MoE parameterization (taking into consideration scaling all of width, depth, expert count, and expert size) based on the principles of μ P and *CompleteP* (Table 1 and Section 3.3) under the auxiliary-loss-free MoE training strategy (Wang et al., 2024) and disentangled (sigmoid) expert weights. We further justify our parameterization via DMFT (Section 4), and report a full suite of empirical results supporting our proposed hyperparameter transfer (Section 5). We point out a few potential future directions left open in our work.

1. As training dynamics in early stages (our 1B scale experiments) versus later stages can be very different, it would be interesting to expand the HP transfer to longer training horizons that are practical.
2. We’d also like to remark that it is not clear whether “compute-optimal” token horizon rules for dense models are practical for MoEs (Clark et al., 2022), as MoEs (a) achieve significantly better performance compared to dense models under the same FLOP budget, so exact conclusions of Chinchilla may not apply and (b) even fixing FLOP, take up significantly more demanding hardware resources (time and memory) due to sparsity. We take our work on HP transfer as a first step to derive scaling law arguments for MoE models in general, at least at a fixed token horizon (see (Clark et al., 2022; Krajewski et al., 2024; Li et al., 2025) for prior literature on fitted MoE scaling laws in different settings).
3. Finally, we left out discussions of other hyperparameters such as batch size, Adam betas, and LR scheduling, all of which are often heavily interconnected and can have a more significant impact as data scale expands.

References

Bergsma, S., Dey, N., Gosal, G., Gray, G., Soboleva, D., and Hestness, J. Power lines: Scaling laws for weight decay and batch size in llm pre-training, 2025a. URL <https://arxiv.org/abs/2505.13738>.

Bergsma, S., Zhang, B. C., Dey, N., Muhammad, S., Gosal, G., and Hestness, J. Scaling with collapse: Efficient and predictable training of llm families. *arXiv preprint arXiv:2509.25087*, 2025b.

Bernstein, J., Wang, Y.-X., Azizzadenesheli, K., and Anandkumar, A. signsdg: Compressed optimisation for non-convex problems. In *International conference on machine learning*, pp. 560–569. PMLR, 2018.

Boix-Adsera, E. and Rigollet, P. The power of fine-grained experts: Granularity boosts expressivity in mixture of experts, 2025. URL <https://arxiv.org/abs/2505.06839>.

Bordelon, B. and Pehlevan, C. Self-consistent dynamical field theory of kernel evolution in wide neural networks. *Advances in Neural Information Processing Systems*, 35: 32240–32256, 2022.

Bordelon, B. and Pehlevan, C. Deep linear network training dynamics from random initialization: Data, width, depth, and hyperparameter transfer, 2025. URL <https://arxiv.org/abs/2502.02531>.

Bordelon, B. and Pehlevan, C. Disordered dynamics in high dimensions: Connections to random matrices and machine learning. *arXiv preprint arXiv:2601.01010*, 2026.

Bordelon, B., Noci, L., Li, M. B., Hanin, B., and Pehlevan, C. Depthwise hyperparameter transfer in residual networks: Dynamics and scaling limit. *arXiv preprint arXiv:2309.16620*, 2023.

Bordelon, B., Chaudhry, H., and Pehlevan, C. Infinite limits of multi-head transformer dynamics. *Advances in Neural Information Processing Systems*, 37:35824–35878, 2024.

Chizat, L. The hidden width of deep resnets: Tight error bounds and phase diagrams, 2025. URL <https://arxiv.org/abs/2509.10167>.

Chizat, L., Oyallon, E., and Bach, F. On lazy training in differentiable programming. *Advances in neural information processing systems*, 32, 2019.

Clark, A., de las Casas, D., Guy, A., Mensch, A., Paganini, M., Hoffmann, J., Damoc, B., Hechtman, B., Cai, T., Borgeaud, S., van den Driessche, G., Rutherford, E., Hennigan, T., Johnson, M., Millican, K., Cassirer, A., Jones, C., Buchatskaya, E., Budden, D., Sifre, L., Osindero, S., Vinyals, O., Rae, J., Elsen, E., Kavukcuoglu, U., and Pehlevan, C. The dynamics of deep learning: A unified framework. *arXiv preprint arXiv:2505.13738*, 2025a.

K., and Simonyan, K. Unified scaling laws for routed language models, 2022. URL <https://arxiv.org/abs/2202.01169>.

Crisanti, A. and Sompolinsky, H. Path integral approach to random neural networks. *arXiv preprint arXiv:1809.06042*, 2018.

Dai, D., Deng, C., Zhao, C., Xu, R., Gao, H., Chen, D., Li, J., Zeng, W., Yu, X., Wu, Y., et al. Deepseekmoe: Towards ultimate expert specialization in mixture-of-experts language models. *arXiv preprint arXiv:2401.06066*, 2024.

Defazio, A. Why gradients rapidly increase near the end of training, 2025. URL <https://arxiv.org/abs/2506.02285>.

Dey, N. S., Zhang, B. C., Noci, L., Li, M., Bordelon, B., Bergsma, S., Pehlevan, C., Hanin, B., and Hestness, J. Don't be lazy: Completeness enables compute-efficient deep transformers. In *The Thirty-ninth Annual Conference on Neural Information Processing Systems*, 2025. URL <https://openreview.net/forum?id=1MU2kaMAN1>.

Dinan, E., Yaida, S., and Zhang, S. Effective theory of transformers at initialization. *arXiv preprint arXiv:2304.02034*, 2023.

Everett, K., Xiao, L., Wortsman, M., Alemi, A. A., Novak, R., Liu, P. J., Gur, I., Sohl-Dickstein, J., Kaelbling, L. P., Lee, J., and Pennington, J. Scaling exponents across parameterizations and optimizers, 2024. URL <https://arxiv.org/abs/2407.05872>.

Fedus, W., Zoph, B., and Shazeer, N. Switch transformers: Scaling to trillion parameter models with simple and efficient sparsity, 2022. URL <https://arxiv.org/abs/2101.03961>.

Ghosh, N., Wu, D., and Bietti, A. Understanding the mechanisms of fast hyperparameter transfer, 2025. URL <https://arxiv.org/abs/2512.22768>.

Hayou, S., Doucet, A., and Rousseau, J. Exact convergence rates of the neural tangent kernel in the large depth limit, 2022. URL <https://arxiv.org/abs/1905.13654>.

He, X. O. Mixture of a million experts, 2024. URL <https://arxiv.org/abs/2407.04153>.

Hestness, J., Narang, S., Ardalani, N., Diamos, G., Jun, H., Kianinejad, H., Patwary, M. M. A., Yang, Y., and Zhou, Y. Deep learning scaling is predictable, empirically. *arXiv preprint arXiv:1712.00409*, 2017.

Hoffmann, J., Borgeaud, S., Mensch, A., Buchatskaya, E., Cai, T., Rutherford, E., de Las Casas, D., Hendricks, L. A., Welbl, J., Clark, A., Hennigan, T., Noland, E., Millican, K., van den Driessche, G., Damoc, B., Guy, A., Osindero, S., Simonyan, K., Elsen, E., Rae, J. W., Vinyals, O., and Sifre, L. Training compute-optimal large language models, 2022. URL <https://arxiv.org/abs/2203.15556>.

Hron, J., Bahri, Y., Sohl-Dickstein, J., and Novak, R. Infinite attention: Nngp and ntk for deep attention networks. In *International Conference on Machine Learning*, pp. 4376–4386. PMLR, 2020.

Jacot, A., Gabriel, F., and Hongler, C. Neural tangent kernel: Convergence and generalization in neural networks, 2020. URL <https://arxiv.org/abs/1806.07572>.

Jiang, A. Q., Sablayrolles, A., Roux, A., Mensch, A., Savary, B., Bamford, C., Chaplot, D. S., de las Casas, D., Hanna, E. B., Bressand, F., Lengyel, G., Bour, G., Lample, G., Lavaud, L. R., Saulnier, L., Lachaux, M.-A., Stock, P., Subramanian, S., Yang, S., Antoniak, S., Scao, T. L., Gervet, T., Lavril, T., Wang, T., Lacroix, T., and Sayed, W. E. Mixtral of experts, 2024. URL <https://arxiv.org/abs/2401.04088>.

Jordan, K. and contributors. Modded-nanogpt. <https://github.com/KellerJordan/modded-nanogpt>, 2025.

Kaplan, J., McCandlish, S., Henighan, T., Brown, T. B., Chess, B., Child, R., Gray, S., Radford, A., Wu, J., and Amodei, D. Scaling laws for neural language models, 2020. URL <https://arxiv.org/abs/2001.08361>.

Karpathy, A. Nanogpt. <https://github.com/karpathy/nanogpt>, 2023.

Kingma, D. P. and Ba, J. Adam: A method for stochastic optimization, 2017. URL <https://arxiv.org/abs/1412.6980>.

Kosson, A., Welborn, J., Liu, Y., Jaggi, M., and Chen, X. Weight decay may matter more than mup for learning rate transfer in practice. *arXiv preprint arXiv:2510.19093*, 2025.

Krajewski, J., Ludziejewski, J., Adamczewski, K., Pióro, M., Krutul, M., Antoniak, S., Ciebiera, K., Król, K., Odrzygóźdż, T., Sankowski, P., et al. Scaling laws for fine-grained mixture of experts. *arXiv preprint arXiv:2402.07871*, 2024.

Large, T., Liu, Y., Huh, M., Bahng, H., Isola, P., and Bernstein, J. Scalable optimization in the modular norm. *Advances in Neural Information Processing Systems*, 37: 73501–73548, 2024.

Lepikhin, D., Lee, H., Xu, Y., Chen, D., Firat, O., Huang, Y., Krikun, M., Shazeer, N., and Chen, Z. Gshard: Scaling giant models with conditional computation and automatic sharding, 2020. URL <https://arxiv.org/abs/2006.16668>.

Li, H., Zheng, W., Wang, Q., Zhang, H., Wang, Z., Xuyang, S., Fan, Y., Ding, Z., Wang, H., Ding, N., Zhou, S., Zhang, X., and Jiang, D. Predictable scale: Part i, step law – optimal hyperparameter scaling law in large language model pretraining, 2025. URL <https://arxiv.org/abs/2503.04715>.

Liu, A., Feng, B., Xue, B., Wang, B., Wu, B., Lu, C., Zhao, C., Deng, C., Zhang, C., Ruan, C., et al. Deepseek-v3 technical report. *arXiv preprint arXiv:2412.19437*, 2024. URL <https://arxiv.org/abs/2412.19437>.

Loshchilov, I. and Hutter, F. Decoupled weight decay regularization, 2019. URL <https://arxiv.org/abs/1711.05101>.

Malasnicki, J., Ciebiera, K., Borun, M., Pioro, M., Ludziejewski, J., Stefaniak, M., Krutul, M., Jaszczur, S., Cygan, M., Adamczewski, K., and Krajewski, J. mu-parameterization for mixture of experts, 2025. URL <https://arxiv.org/abs/2508.09752>.

Mei, S., Montanari, A., and Nguyen, P.-M. A mean field view of the landscape of two-layer neural networks. *Proceedings of the National Academy of Sciences*, 115(33):E7665–E7671, 2018.

Mignacco, F., Krzakala, F., Urbani, P., and Zdeborová, L. Dynamical mean-field theory for stochastic gradient descent in gaussian mixture classification. *Advances in Neural Information Processing Systems*, 33:9540–9550, 2020.

Młodożeniec, B., Ablin, P., Béthune, L., Busbridge, D., Klein, M., Ramapuram, J., and Cuturi, M. Completed hyperparameter transfer across modules, width, depth, batch and duration, 2025. URL <https://arxiv.org/abs/2512.22382>.

Penedo, G., Kydlíček, H., allal, L. B., Lozhkov, A., Mitchell, M., Raffel, C., Werra, L. V., and Wolf, T. The fineweb datasets: Decanting the web for the finest text data at scale, 2024. URL <https://arxiv.org/abs/2406.17557>.

Qiu, S., Xiao, L., Wilson, A. G., Pennington, J., and Agarwala, A. Scaling collapse reveals universal dynamics in compute-optimally trained neural networks, 2025. URL <https://arxiv.org/abs/2507.02119>.

Radford, A., Wu, J., Child, R., Luan, D., Amodei, D., Sutskever, I., et al. Language models are unsupervised multitask learners. *OpenAI technical report*, 2019.

Raffel, C., Shazeer, N., Roberts, A., Lee, K., Narang, S., Matena, M., Zhou, Y., Li, W., and Liu, P. J. Exploring the limits of transfer learning with a unified text-to-text transformer. *Journal of machine learning research*, 21(140):1–67, 2020. URL <https://arxiv.org/abs/1910.10683>.

Roberts, D. A., Yaida, S., and Hanin, B. *The principles of deep learning theory*, volume 46. Cambridge University Press Cambridge, MA, USA, 2022.

Rotskoff, G. and Vanden-Eijnden, E. Trainability and accuracy of artificial neural networks: An interacting particle system approach. *Communications on Pure and Applied Mathematics*, 75(9):1889–1935, 2022.

Shazeer, N., Mirhoseini, A., Maziarz, K., Davis, A., Le, Q., Hinton, G., and Dean, J. Outrageously large neural networks: The sparsely-gated mixture-of-experts layer. In *International Conference on Learning Representations*, 2017. URL <https://openreview.net/forum?id=B1ckMDq1g>.

StepFun et al. Step-3 is large yet affordable: Model-system co-design for cost-effective decoding, 2025. URL <https://arxiv.org/abs/2507.19427>.

Su, Z., Li, Q., Zhang, H., Ye, W., Xue, Q., Qian, Y., Xie, Y., Wong, N., and Yuan, K. Unveiling super experts in mixture-of-experts large language models, 2025. URL <https://arxiv.org/abs/2507.23279>.

Wang, L., Gao, H., Zhao, C., Sun, X., and Dai, D. Auxiliary-loss-free load balancing strategy for mixture-of-experts. *arXiv preprint arXiv:2408.15664*, 2024. URL <https://arxiv.org/abs/2408.15664>.

Wang, X. and Aitchison, L. How to set adamw’s weight decay as you scale model and dataset size, 2025. URL <https://arxiv.org/abs/2405.13698>.

Wen, K., Hall, D., Ma, T., and Liang, P. Fantastic pretraining optimizers and where to find them, 2025. URL <https://arxiv.org/abs/2509.02046>.

Yaida, S. Meta-principled family of hyperparameter scaling strategies. *arXiv preprint arXiv:2210.04909*, 2022.

Yang, G. and Hu, E. J. Feature learning in infinite-width neural networks, 2022. URL <https://arxiv.org/abs/2011.14522>.

Yang, G., Hu, E. J., Babuschkin, I., Sidor, S., Liu, X., Farhi, D., Ryder, N., Pachocki, J., Chen, W., and Gao, J. Tensor programs v: Tuning large neural networks via zero-shot hyperparameter transfer, 2022. URL <https://arxiv.org/abs/2203.03466>.

Yang, G., Simon, J. B., and Bernstein, J. A spectral condition for feature learning. *arXiv preprint arXiv:2310.17813*, 2023a. URL <https://arxiv.org/abs/2310.17813>.

Yang, G., Yu, D., Zhu, C., and Hayou, S. Tensor programs vi: Feature learning in infinite-depth neural networks, 2023b. URL <https://arxiv.org/abs/2310.02244>.

Zhou, Y., Lei, T., Liu, H., Du, N., Huang, Y., Zhao, V., Dai, A., Chen, Z., Le, Q., and Laudon, J. Mixture-of-experts with expert choice routing, 2022. URL <https://arxiv.org/abs/2202.09368>.

Zhou, Y., Xing, S., Huang, J., Qiu, X., and Guo, Q. How to set the learning rate for large-scale pre-training?, 2026. URL <https://arxiv.org/abs/2601.05049>.

Zoph, B., Bello, I., Kumar, S., Du, N., Huang, Y., Dean, J., Shazeer, N., and Fedus, W. St-moe: Designing stable and transferable sparse expert models, 2022. URL <https://arxiv.org/abs/2202.08906>.

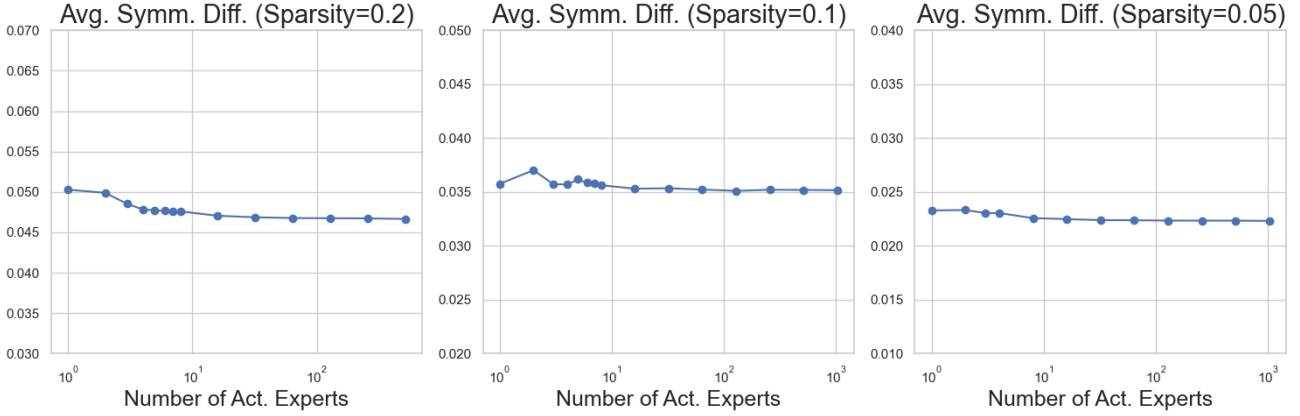


Figure 6. (Appendix B) Justification for how constant LR for biases enables constant symmetric difference in activation sets per step update. We see that under random activations, keeping a constant expert bias LR preserves (across scaling total expert count while fixing sparsity) the average symmetric difference of activated expert proportion per step.

A. More experiment details

In this section we lay-out some further experiment details from Section 5. We train decoder-only MoE models described in Section 3.1. Our attention, embedding, and normalization setups are based on the public Nano-GPT repo (Karpathy, 2023) and standard GPT-2 style tokenizer (Radford et al., 2019) with a vocabulary size of 50304. For all optimization, we use standard Adam betas $\beta_1, \beta_2 = 0.9, 0.95$ and a negligible Adam $\varepsilon = 10^{-12}$. We use a fixed $d_{\text{head}} = 64$ (while scaling $\text{num_head} \propto n_{\text{embd}}$ for large embedding width) for multi-head self-attention following (Dey et al., 2025). We use QK^T/d_{head} (as opposed to standard $\sqrt{d_{\text{head}}}$) for the normalization of self-attention following (Yang et al., 2022). For experiments with scaling models, our base model has dimensions of base $n_{\text{embd}} = 512$, base $\alpha_{\text{ffn}} = 1$, base $L = 8$, and we up-scale relevant multipliers via the prescribed parametrization in Table 1 (we point our parameterizations for all non-FFN HPs and LN HPs to Table 1 in (Dey et al., 2025)). We train our models using the standard autoregressive cross-entropy loss (i.e. the next token prediction objective) and always report the log perplexity score. As with the standard Nano-GPT (Karpathy, 2023) setup, we use pre-LayerNorm, tied embeddings, absolute learned position embeddings, and GELU nonlinearity. Because router matrices takes up $O(n_{\text{embd}}^{-1})$ fraction of total FFN parameter counts, we may ignore them and derive total parameters as

$$P_{\text{total}} \approx n_{\text{embd}}^2 \cdot L \cdot (4 + 2 \cdot n_{\text{exp}} \cdot \alpha_{\text{ffn}}) + n_{\text{embd}} \cdot (1024 + 50304)$$

where 1024 is the context length and 50304 is the vocabulary size, and for active parameters

$$P_{\text{active}} \approx n_{\text{embd}}^2 \cdot L \cdot (4 + 2 \cdot n_{\text{act}} \cdot \alpha_{\text{ffn}}) + n_{\text{embd}} \cdot (1024 + 50304).$$

Our experiments are run on H100s and bit-wise deterministic. See supplementary materials for implementation details.

B. Learning rate for biases

We derive a simple heuristic on why bias learning rate should not be adjusted when scaling the total number of experts while fixing sparsity. Consider the following pseudo-code, where we assume that the pre-activated $\sigma^{-1}(g_i)$'s are i.i.d. Gaussian, (existing) biases are uniformly distributed in a fixed range, and updated biases are uniformly distributed in a fixed range. This represents the training phase where load imbalance is $\Theta(1)$ proportion of total tokens. The goal is that, regardless of the total number of experts, for a fixed set of gradient distribution, a constant bias learning rate enables constant expert activation set change. See comments below for how we set-up the heuristics.

```

active = sparsity * numExperts
for _ in range(N_TEST):
    logits = 0.02 * np.random.normal(0, 1, numExperts)
    # Assuming random logits, or $r_i$'s, in the main text
    sigLogits = sigmoid(logits)

```

```

bias = 0.05 * np.random.uniform(0, 1, num_experts)
# Assuming random current expert biases
mask_top_a = set(np.argsort(sig_logits+bias)[-active:])
bias_update = 0.01 * np.random.uniform(0, 1, num_experts)
# Assuming random bias updates from load imbalance
mask_top_b = set(np.argsort(sig_logits+bias+bias_update)[-active:])
print(len(mask_top_a & mask_top_b) / active)
    
```

Results of the above snippet with different sparsities and different number of experts are plotted in Figure 6.

C. Weight decay

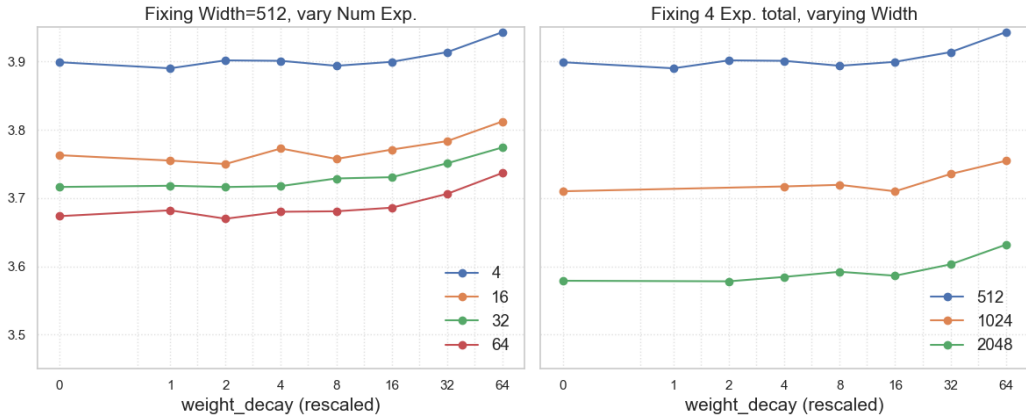


Figure 7. Weight decay with independent scaling preserving $\eta\lambda$ (x-axis here is the re-scaled τ_{EMA}). While we do see preliminary transfer behaviors across model scales when using independent weight decay, we do not observe significant benefit from a nontrivial WD.

While weight decay (WD) is an important hyperparameter in AdamW (Loshchilov & Hutter, 2019), the exact empirical effect in the context of HP transfer is not well understood. For instance, (Kosson et al., 2025) found that independent weight decay, keeping $\eta \cdot \lambda$ constant (across model scales) such that in every step a constant fraction of weights gets whitened, enables HP transfer. On top of that, (Dey et al., 2025) argued that this independent weight decay $\eta\lambda$ may require depth adjustments according to the depth scaling exponent. However, another line of empirical works (Wang & Aitchison, 2025; Bergsma et al., 2025a) suggests that the scaled invariant should be the effective EMA timescale $\tau = T\eta\lambda$ where T is the number of steps trained. This is contradictory with independent weight decay when T is connected to model parameters, such as width or depth (often the practical case for ‘compute-optimality’ (Kaplan et al., 2020)). Finally, works such as (Defazio, 2025) suggested WD scheduling, another variable to be considered.

In our experiments with weight decay in a limited scope, we found that at the 1B token horizon with $T = 2000$ steps, a nontrivial weight decay does not significantly outperform having zero weight decay altogether, and hence all our experiments in the main text are done without weight decay. See Figure 7.

D. Other experiment results

D.1. Constant-scale HP tuning for the base model

In (Yang & Hu, 2022; Yang et al., 2022), the authors pointed out that good HP transfer is crucially based on the ‘close to optimality’ of the scaling. Without specific care, HPs found from tuning small models can be ‘contaminated’ by finite-width effects, which fail to yield useful transfer (Figure 17, (Ghosh et al., 2025)). This motivates tuning constant-scaled multipliers on relevant HPs, whose benefits for dense models were remarked in (Everett et al., 2024; Mlodzeniec et al., 2025; Ghosh et al., 2025) that not only promote better loss (in the base model) but likely contribute to more reliable transfer. In our experiments with MoE layers, we found that balancing constant-scaled hyperparameters not only leads to better performance, but it is specifically crucial for stable training dynamics (across different random seeds) on large learning rates. In practice, we enable two constant multipliers for each MoE parameter groups for learning rate and initialization. While each group of

weights has a three relevant HPs: learning rate, initialization, and multiplier, in the so-called *abc*-parameterization (Yang & Hu, 2022), only *two* degrees of freedom are present. We will take all weight multipliers to be one, so only initializations and learning rates are at play. We report loss results on ablation in Figure 8 and load balancing ablation in Figure 9.

Instead of striving to obtain *the optimal* set of constant-scale HPs across the base model, which is an extremely high dimensional problem and requires exhaustive and expensive tuning even on small models (Młodożeniec et al., 2025), we only aimed for one *stable* set of constants on the base model that enables consistent model behaviors (for larger learning rates beyond the optimal one) and stable training dynamics (loss across seeds), which we found suffices for HP transfer via our parameterization. The goal is to avoid “cut-off” type behaviors (e.g. Figure 8 without constant tuning, see also Figure 13(b) in (Młodożeniec et al., 2025)), where loss immediately diverges above optimal learning rate, in which case one is likely transferring model divergence rather than optimal HP, leading to (a) unreliable transfer conclusions because such divergence can happen probabilistically across seed (Figure 8), (b) unsafe HPs to use being closer to divergence limits (albeit optimal on base models), and (c) likely nontrivial performance left on the table. After tuning, we found that our loss dynamics are stable well beyond optimal LRs.

To tune these constants on the base model, we start from the default (all-one) and sweep over each component sequentially on the base model (fixing global learning rate and initialization), similar to coordinate-descent, and only update when significant improvements across seeds are observed. We ended up with `attn_QKV_lr_mult` = 1/16, `attn_V_init_mult` = 1/16, `router_lr_mult` = 1/16, `mlp_down_init_mult` = 1/4, `mlp_down_lr_mult` = 1/16 (all else being one) in a single pass which gave satisfying base model behaviors already. In our two settings (κ = 1/4 and 1/12), we reused the same set of constant-scale HPs, as we found that the constants tuned from κ = 1/4 worked well to achieve our stability purpose in the κ = 1/12 base model. In fact, in Figure 10, the degradation of stability happens rather slowly as $\kappa \rightarrow 0$ (only at κ = 1/16 do we see marginally unstable behavior). Finally, while we found success in constant tuning for our purposes, application of normalization layers can also be beneficial (Młodożeniec et al., 2025). In our experiments, we take the standard normalizations from (Karpathy, 2023) with learning prescriptions from (Dey et al., 2025) and defer the study of advanced normalization techniques into future work.

D.2. Expert load balancing

We briefly justify our choice of expert load balancing strategy, as opposed to the perhaps more common auxiliary loss type regularization (Shazeer et al., 2017; Lepikhin et al., 2020), where an external penalty L_{load} is computed (summed over each layer of some load violation function) on top the standard cross-entropy (CE) loss, and the model is trained on

$$L_{\text{total}} = L_{\text{CE}} + \alpha L_{\text{load}}$$

for some α . In particular, the object of interest in studying this type of loss is (1) what is a concrete desiderata with respect to load balancing penalty in terms of max-update principles, and (2) whether there exists a suitable parameterization and a fixed scale of α throughout training such that max-update principles will be upheld.

When the backward pass with L_{load} is involved, all parameters receive a gradient from the regularizer. Therefore, a natural choice could be forcing

$$\nabla_W L_{\text{CE}} = \Theta(\nabla_W L_{\text{Load}})$$

for all parameters groups, so that cross-validation loss and load balancing regularization are on the same scale. However, the practical implications may be more complex as (a) the router matrix at each layer is predominantly responsible for the load balancing at this layer, and it is not clear whether it is desirable or not for FFN or self-attention modules to receive the same gradient norm from load balancing (in other layers) as they would from cross-entropy, or if one router matrix in some layer needs to receive gradients from load-balancing other layers. One possible remedy is to restrict per-layer load balancing gradients to only the router matrix of that specific layer, but this seems to deviate from known practices nonetheless.

Furthermore, under the standard Switch-transformer (Fedus et al., 2022) framework with softmax activation, it’s possible for a phase transition where router logits (expert mixing coefficients) go from near uniform (at initialization) to close to one-hot, making designing the desiderata for HP transfer and α scale tricky. Whereas in our case, the un-normalized mixing coefficients g ’s through a sigmoid gate are always bounded and well-behaved.

Finally, when we finally justify HP transfer on training or validation loss, usually the object of study is only concerning cross-entropy and not with the regularized load-balancing loss. It has further been reported (Wang et al., 2024) in some cases that introducing too much auxiliary loss harms performance on cross-entropy loss. The tradeoff for quicker load balance versus validation loss deviates from the pure study of HP transfer and we do not pursue here.

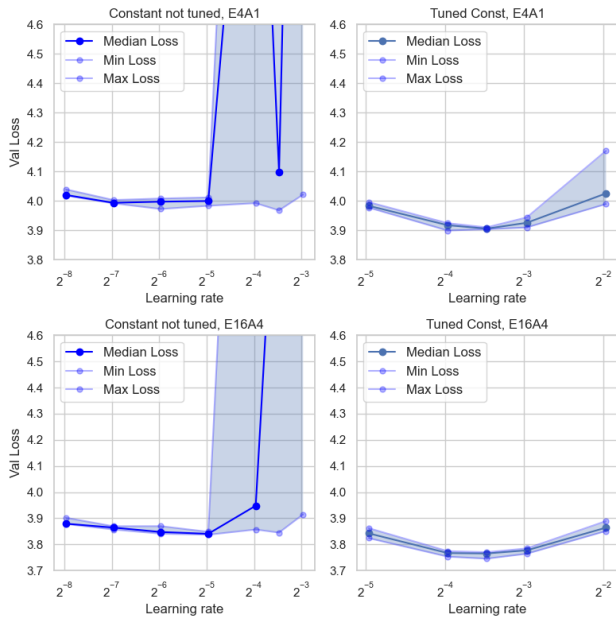


Figure 8. Ablation results on constant tuning, run across 4 different seeds with reported (min, median, max) bars. Default constants (1) have higher loss overall, even on the opt LR from sweeping, and (2) on larger LRs, some seeds converge (and even exhibit good performance), whereas others diverge completely, making LR sweep results unreliable. Further issue with untuned constants in terms of load-balancing is in Figure 9.

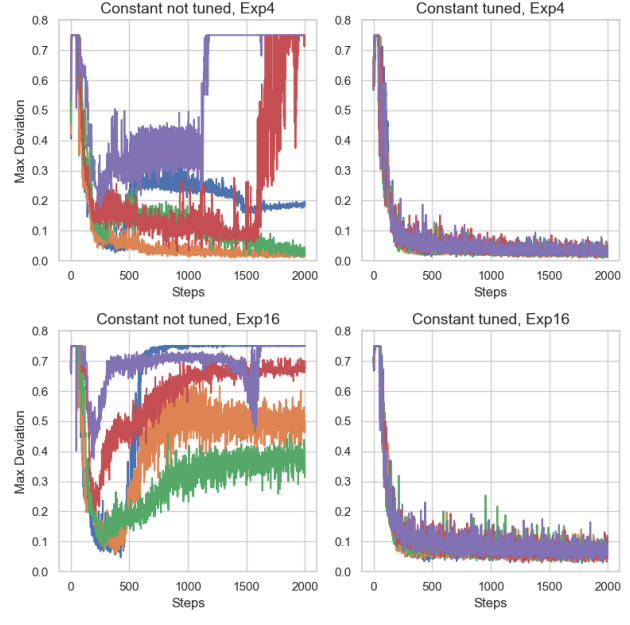


Figure 9. Maximum load deviation in (2) for all experts over all layers (range from 0 to $1 - \kappa = 0.75$) throughout training, where each curve represents a distinct learning rate. We can see that with tuned constants, max load deviation drops very quickly and stays low (across mini-batches), meaning that expert load is balanced effectively. However, for default constants load is not balanced for any learning rate swept. Due to the constant effect of load balancing regularizer in place, a non-balanced expert load can harm model performance and prohibit good transfer.

D.3. More experiments

1. In Figure 11, we run a simple ablation to see that a standard fan-in initialization when scaling α_{ffn} fails loss-scale invariance, whereas our derived α^{-1} rule on expert down projection layers satisfied the invariance.
2. In Figure 12, we fit runs (with optimal HP) in terms of log parameter count and validation loss at the 1B data scale. We find that a linear fit returns remarkable accuracy. In particular, when fitting against the total number of model parameters, the r-squared coefficient (with validation loss) for total parameters and non-embedding number of parameters are 0.900 and 0.914. When fitting against *activated* number of parameters, total activated r-square is lowered to 0.844 whereas non-embedding fit r-squared slightly increased to 0.933.
3. In Figure 13, we run a few other LR sweeps (with fixed 1B token count) varying different types of hyperparameter configurations scaling expert count and width together. In experiments up to 2.54B models (50x base) and a full 10% loss gap from base model, we see that transfer holds well.
4. In Figure 14, we test transfer on GPT2-small (124M) with 2.5B total number of tokens (20 tokens per activated parameter), with a sparsity $\kappa = 1/4$ similar to the style of Figure 1. Both learning rate and initialization scale transfer holds up at the larger token horizon.
5. In Figure 15, we compare our results ran on GPT2-medium (355M). While recorded (Jordan & contributors, 2025) Speedrun logs for this architecture only exist after the 124M base variant was highly optimized (which vastly improves Figure 1), we still manage to outperform the (tuned) llm.c baseline (Karpathy, 2023) easily.
6. In Figure 16, we see that the tradeoff in Figure 5 (Finding 3.1 in the main text) persists for over-trained models (having 50M and 100M active parameters trained on close to 5B tokens).
7. In Figure 17, we report the maximum expert load imbalance across the entire model. We see that even when we scale up number of experts, the maximum load imbalance across all experts in all layers converges to uniform.

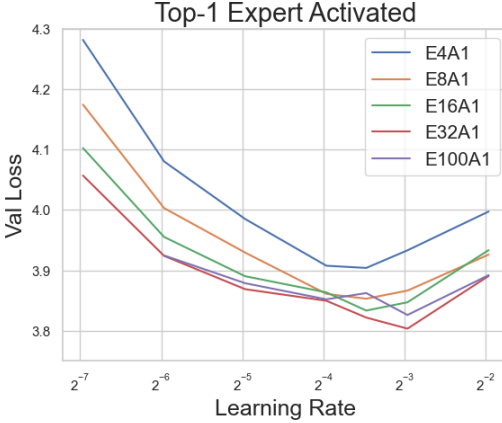


Figure 10. Section 3.2: Optimal LR does not transfer in our setting when fixing activating top-1 expert and scaling the number of total experts ($\kappa \rightarrow 0$). Constant-scaled hyperparameters (Apdx. D.1) also fail transfer of stability as evidenced by E100A1.

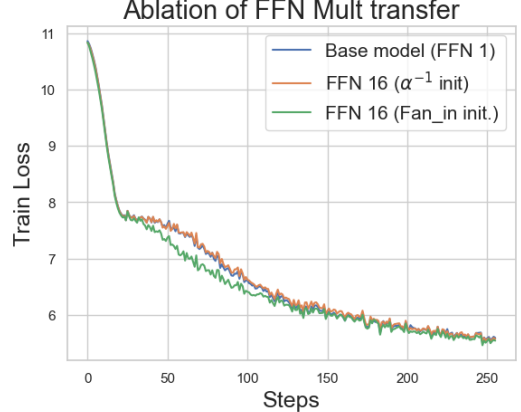


Figure 11. The standard fan-in initialization ($\sigma_{dn} \sim \alpha_{ffn}^{-1/2}$) for expert down projection fails early-loss scaling invariance when α_{ffn} scales. See Section 3.3 for our derivation to α_{ffn}^{-1} and Figure 3.

E. Dynamical mean field theory

In this section, we derive the dynamical mean field theory equations for the large width, large expert count, and large depth limit of this model. We assume a deep residual network consisting of L MoE layers without attention. We further focus on gradient flow in the present analysis but this can be easily relaxed to discrete time SGD (Bordelon & Pehlevan, 2022; Bordelon et al., 2023).

Notation. For simplicity of notations, we denote in the below:

$$K \triangleq n_{act}, \quad E \triangleq n_{exp}, \quad N \triangleq n_{embd}, \quad N_e \triangleq \alpha_{ffn} \cdot n_{embd} = n_{hid}.$$

We will use $\langle \rangle$ to represent the residual stream neuron average. We will use $[\cdot]$ for expert average and $\{\cdot\}$ to represent the within-expert neuron average. A covariance kernel will be represented as $C_{ab}^\ell(\mathbf{x}, \mathbf{x}', t, t') = \langle a^\ell(\mathbf{x}, t) b^\ell(\mathbf{x}', t') \rangle$ and response functions $R_{ab}^\ell(\mathbf{x}, \mathbf{x}', t, t') = \left\langle \frac{\delta a^\ell(\mathbf{x}, t)}{\delta b^\ell(\mathbf{x}', t')} \right\rangle$. Lastly we will use M_{ab}^ℓ to represent mixture kernels which are expert averages over within-expert variables such as $M_{\dot{\sigma}, \mathcal{A}, \mathcal{A}}^\ell(\mathbf{x}, \mathbf{x}', t, t') = [\dot{\sigma}^\ell(\mathbf{x}, t) \dot{\sigma}^\ell(\mathbf{x}', t') \mathcal{A}^\ell(\mathbf{x}, t) \mathcal{A}^\ell(\mathbf{x}', t')]$. Where appropriate, we will often drop indices over \mathbf{x} and t and use notation like $\chi^\ell \hat{\chi}^\ell$ instead of $\int d\mathbf{x} dt \chi^\ell(\mathbf{x}, t) \hat{\chi}^\ell(\mathbf{x}, t)$. Our DMFT forward pass notations, as carefully defined below, will be slightly different from Section 3.1 in the main text.

Defining the Moment Generating Function Let $f(\mathbf{x}, t)$ represent the output of the neural network. We initialize every random initial weight to have unit variance except \mathbf{r}_k will be initialized at zero (but the biases are non-zero)².

$$Z = \left\langle \exp \left(N \int dt d\mathbf{x}' f(\mathbf{x}, t) \hat{f}(\mathbf{x}, t) \right) \right\rangle \quad (5)$$

We introduce the definition of the network function $f(\mathbf{x}, t)$ and intermediate variables

$$f(\mathbf{x}, t) = \frac{1}{\gamma_0 N} \mathbf{w}^L(t) \cdot \mathbf{h}^L(\mathbf{x}, t) \quad (6)$$

²This will not change the limiting dynamics since the $\frac{1}{N} \mathbf{r}_k(0) \cdot \mathbf{h}$ will have subleading variance and no response function in the limiting DMFT. Rather, we rely on the random initial biases $b_k(0)$ to generate diversity across experts at initialization.

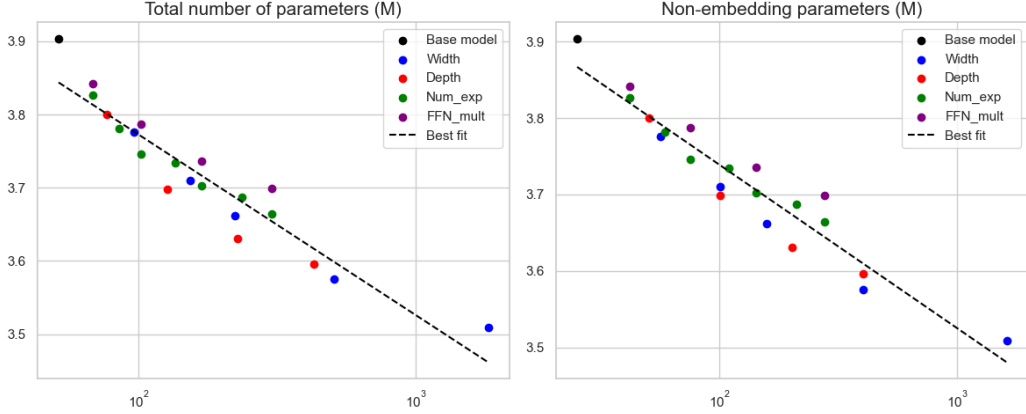


Figure 12. We plot model final validation loss versus model size, when scaling different dimensions at the 1B scale (left: total parameters, right: number of non-embedding parameters), we see that the number of non-embedding parameters (in log-scale) is more linearly correlated with final loss.

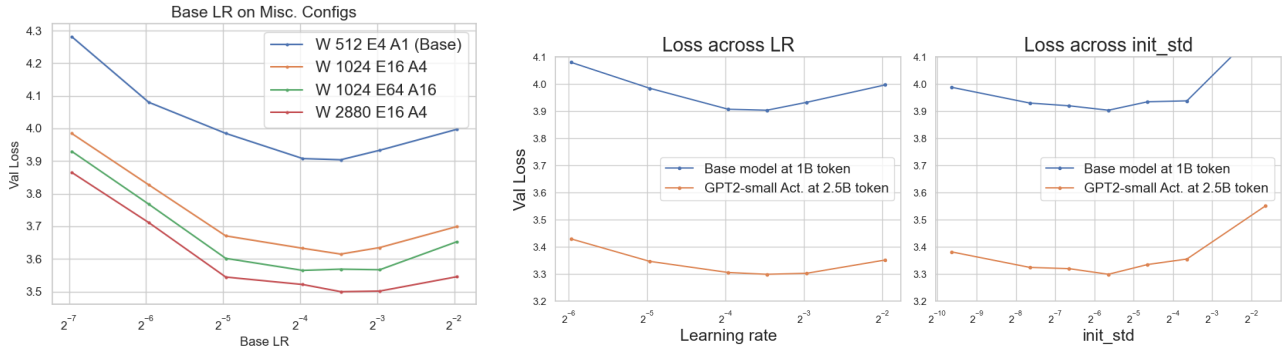


Figure 13. Base LR transfer on 1B token when scaling up miscellaneous configurations together (depth 8, α_1). The largest model taken here has 2.54B total number of parameters and 944M activated.

Figure 14. Transfer from base model (1B fixed token) to GPT2-small-124M (with 4 experts, 1 activated, and hidden multiplier 4.0) trained at 20TPP (2.5B token) with no weight decay and cosine LR decay to zero.

where the hidden features $\mathbf{h}^\ell(\mathbf{x}, t)$ are determined by the forward pass recursion

$$\begin{aligned}
 \mathbf{h}^{\ell+1}(\mathbf{x}, t) &= \mathbf{h}^\ell(\mathbf{x}, t) + \frac{\sqrt{N}}{LN_e E} \sum_{k=1}^E \sigma_k(\mathbf{x}, t) \mathbf{W}_k^{\ell,2}(t) \phi(\mathbf{h}_k^\ell(\mathbf{x}, t)) \\
 &= \mathbf{h}^\ell(\mathbf{x}, t) + \underbrace{\frac{1}{L} \frac{\sqrt{N}}{N_e E} \sum_{k=1}^E \sigma_k(\mathbf{x}, t) \mathbf{W}_k^{\ell,2}(0) \phi(\mathbf{h}_k^\ell(\mathbf{x}, t))}_{\bar{\chi}^\ell(\mathbf{x}, t)} \\
 &\quad + \gamma_0 \mathbb{E}_{\mathbf{x}'} \underbrace{\int dt' \left(\frac{1}{E} \sum_k \sigma_k(\mathbf{x}, t) \sigma_k(\mathbf{x}', t') C_{\phi, k}^{\ell,1}(\mathbf{x}, \mathbf{x}', t, t') \right) \mathbf{g}^{\ell+1}(\mathbf{x}', t')}_{M_{\sigma \sigma C_\phi}^\ell(\mathbf{x}, \mathbf{x}', t, t')} \\
 \mathbf{h}_k^\ell(\mathbf{x}, t) &= \frac{1}{\sqrt{N}} \mathbf{W}_k^{\ell,1}(t) \mathbf{h}^\ell(\mathbf{x}, t) \\
 &= \underbrace{\frac{1}{\sqrt{N}} \mathbf{W}_k^{\ell,1}(0) \mathbf{h}^\ell(\mathbf{x}, t)}_{\chi_k^{\ell,1}(\mathbf{x}, t)} + \underbrace{\gamma_0 \mathbb{E}_{\mathbf{x}'} \int dt' \left(\frac{1}{N} \mathbf{h}^\ell(\mathbf{x}, t) \cdot \mathbf{h}^\ell(\mathbf{x}', t') \right) \sigma_k(\mathbf{x}', t') \mathbf{g}_k^\ell(\mathbf{x}', t')}_{C_h^\ell(\mathbf{x}, \mathbf{x}', t, t')} \tag{7}
 \end{aligned}$$

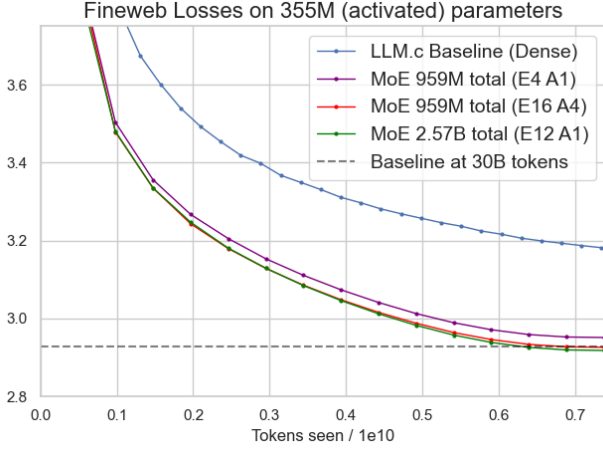


Figure 15. Fixing GPT2-medium 355M activated, we compare our scaled MoE models (again zero-shot HP from 38M active base model) under two different sparsity settings (and two different expert size multipliers for $\kappa = 1/4$). Under the same total and activated parameter count, E4A1 significantly underperforms E16A4, which performs similarly to E12A1, despite the latter being larger.

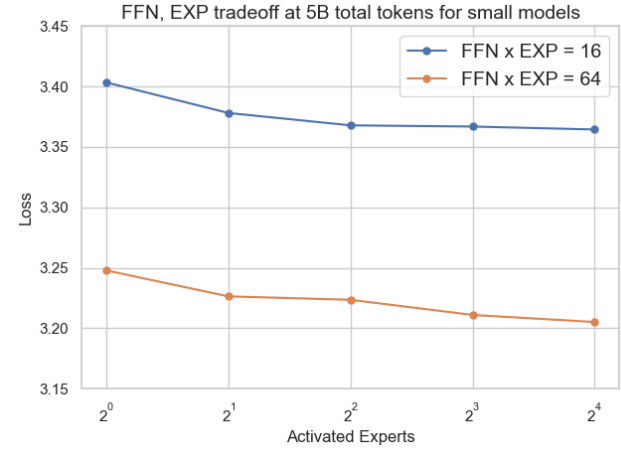


Figure 16. Smaller models (51M and 102M activated) trained on a much longer token horizon (4.92B tokens). We see that having a larger number of smaller experts still consistently yield benefit over fewer large experts.

Similarly, for the backward pass variables $\mathbf{g}^\ell = N\gamma_0 \frac{\partial f(\mathbf{x}, t)}{\partial \mathbf{h}^\ell(\mathbf{x}, t)}$ we have

$$\mathbf{g}^\ell(\mathbf{x}, t) = \mathbf{g}^{\ell+1}(\mathbf{x}, t) + \frac{\sqrt{N}}{LN_e E} \sum_k \sigma_k(\mathbf{x}, t) \mathbf{W}_k^{\ell,1}(t)^\top \mathbf{g}_k^{\ell,1}(\mathbf{x}, t) \quad (8)$$

$$+ \frac{1}{LE} \sum_k \dot{\sigma}_k(\mathbf{x}, t) \mathcal{A}_k(\mathbf{x}, t) \mathbf{r}_k(t) \quad (9)$$

$$= \mathbf{g}^{\ell+1}(\mathbf{x}, t) + \underbrace{\frac{\sqrt{N}}{LN_e E} \sum_k \sigma_k(\mathbf{x}, t) \mathbf{W}_k^{\ell,1}(0)^\top \mathbf{g}_k^{\ell,1}(\mathbf{x}, t)}_{\bar{\xi}^\ell(\mathbf{x}, t)} \quad (10)$$

$$+ \frac{\gamma_0}{L} \mathbb{E}_{\mathbf{x}'} \int dt' \Delta(\mathbf{x}', t') \underbrace{\left(\frac{1}{E} \sum_k \sigma_k^\ell(\mathbf{x}, t) \sigma_k^\ell(\mathbf{x}', t') C_{g_k}^{\ell,1}(\mathbf{x}, \mathbf{x}', t, t') \right) \mathbf{h}^\ell(\mathbf{x}', t')}_{M_{\sigma \sigma C_g}^\ell} \quad (11)$$

$$+ \frac{\gamma_0}{L} \mathbb{E}_{\mathbf{x}'} \int dt' \Delta(\mathbf{x}', t') \underbrace{\left(\frac{1}{E} \sum_k \dot{\sigma}(\mathbf{x}, t) \dot{\sigma}(\mathbf{x}', t') \mathcal{A}_k(\mathbf{x}, t) \mathcal{A}_k(\mathbf{x}', t') \right) \mathbf{h}^\ell(\mathbf{x}', t')}_{M_{\dot{\sigma} \dot{\sigma} \mathcal{A} \mathcal{A}}^\ell} \quad (12)$$

Further, we have the intermediate gradient fields

$$\mathbf{g}_k^{\ell,1}(\mathbf{x}, t) = \dot{\phi}(\mathbf{h}_k^{\ell,1}(\mathbf{x}, t)) \odot \mathbf{z}_k^{\ell,1}(\mathbf{x}, t) \quad (13)$$

$$\mathbf{z}_k^{\ell,1}(\mathbf{x}, t) = \frac{1}{\sqrt{N}} \mathbf{W}_k^{\ell,2}(t)^\top \mathbf{g}^{\ell+1}(\mathbf{x}, t) \quad (14)$$

$$= \underbrace{\frac{1}{\sqrt{N}} \mathbf{W}_k^{\ell,2}(0)^\top \mathbf{g}^{\ell+1}(\mathbf{x}, t)}_{\xi_k^{\ell,1}(\mathbf{x}, t)} + \gamma_0 \mathbb{E}_{\mathbf{x}'} \int dt' \Delta(\mathbf{x}', t') C_g^{\ell+1}(\mathbf{x}, \mathbf{x}', t, t') \phi(\mathbf{h}_k^{\ell,1}(\mathbf{x}', t')) \quad (15)$$

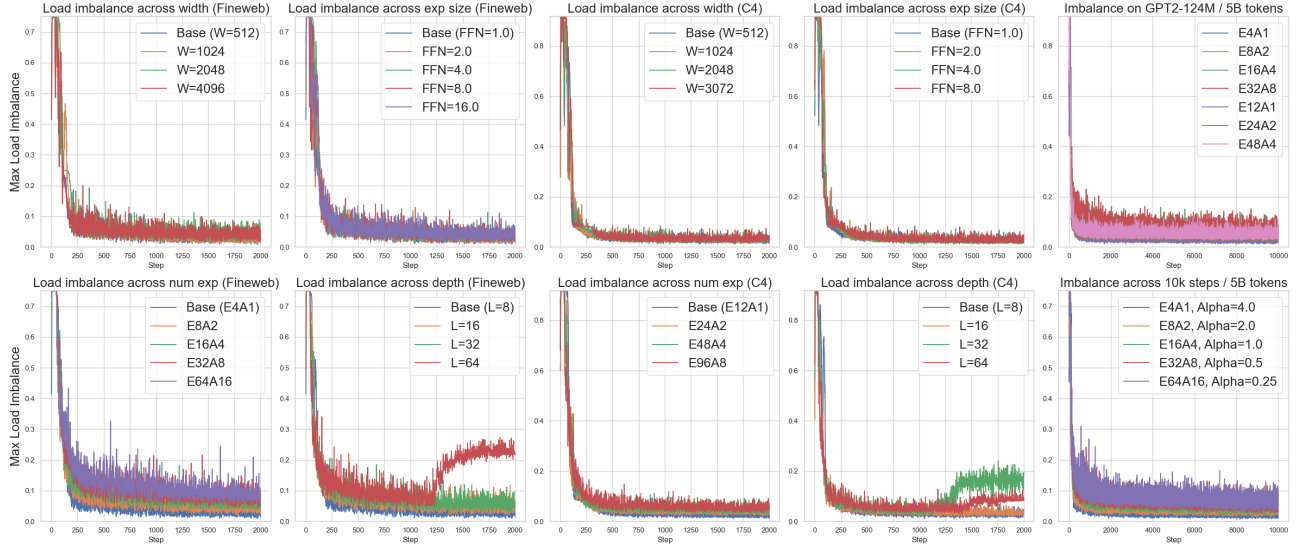


Figure 17. Maximum load imbalance in our class of scaling models. Load imbalance (Eqn. 2) is calculated as the max, over $L \cdot n_{\text{embd}}$ total experts in the model, absolute value of (proportion of tokens routed to the expert) subtracts (the target uniform sparsity κ), similar to Figure 9. Here y -axis is from 0 to $1 - \kappa$. We observe that load balancing convergence is perfect when we increase width and expert size, the number of experts per layer, but may be compromised when we scale up depth for too large, which we hypothesize is due to constant-HP tuning issues and may require further investigation (the same hypothesis bars us from reproducing reliable loss collapse in early steps for Figure 3 when scaling number of layers). The last column shows that load balance convergence persists even when training horizon is extended.

We expand out the dynamics

$$\begin{aligned}
 p_k^\ell(\mathbf{x}, t) &= \gamma_0 \mathbb{E}_{\mathbf{x}'} \int dt' \Delta(\mathbf{x}', t') \mathcal{A}_k^\ell(\mathbf{x}', t') \dot{\sigma}_k(\mathbf{x}', t') C_h^\ell(\mathbf{x}, \mathbf{x}', t, t') \\
 \mathcal{A}_k^\ell(\mathbf{x}, t) &= \frac{1}{\sqrt{N} N_e} \mathbf{g}^{\ell+1}(\mathbf{x}, t)^\top \mathbf{W}_k^{\ell,2}(0) \phi(\boldsymbol{\eta}_k^\ell(\mathbf{x}, t)) + \gamma_0 \mathbb{E}_{\mathbf{x}'} \int dt' \sigma_k(\mathbf{x}', t') C_g^{\ell+1}(\mathbf{x}, \mathbf{x}', t, t') C_{\phi_k^1}^\ell(\mathbf{x}, \mathbf{x}', t, t') \\
 &= \underbrace{\frac{1}{N_e} \boldsymbol{\xi}_k^{\ell,1}(\mathbf{x}, t) \cdot \phi(\mathbf{h}_k^{\ell,1}(\mathbf{x}, t))}_{C_{\xi_k}^\ell} + \gamma_0 \mathbb{E}_{\mathbf{x}'} \int dt' \sigma_k(\mathbf{x}', t') C_g^{\ell+1}(\mathbf{x}, \mathbf{x}', t, t') C_{\phi_k^1}^\ell(\mathbf{x}, \mathbf{x}', t, t') \quad (16)
 \end{aligned}$$

The only random variables that depend on the random weights that we need to characterize are

$$\boldsymbol{\chi}_k^{\ell,1}(\mathbf{x}, t) = \frac{1}{\sqrt{N}} \mathbf{W}_k^{\ell,1}(0) \mathbf{h}^\ell(\mathbf{x}, t), \quad \bar{\boldsymbol{\chi}}^{\ell+1}(\mathbf{x}, t) = \frac{\sqrt{N}}{N_e E} \sum_{k=1}^E \sigma_k(\mathbf{x}, t) \mathbf{W}_k^{\ell,2}(0) \phi(\mathbf{h}_k^{\ell,1}(\mathbf{x}, t)) \quad (17)$$

$$\boldsymbol{\xi}_k^{\ell,1}(\mathbf{x}, t) = \frac{1}{\sqrt{N}} \mathbf{W}_k^{\ell,2}(0)^\top \mathbf{g}^{\ell+1}(\mathbf{x}, t), \quad \bar{\boldsymbol{\xi}}^\ell(\mathbf{x}, t) = \frac{\sqrt{N}}{N_e E} \sum_{k=1}^E \sigma_k(\mathbf{x}, t) \mathbf{W}_k^{\ell,1}(0)^\top \mathbf{g}_k^{\ell,1}(\mathbf{x}, t) \quad (18)$$

The global order parameters we will track include the following correlation kernels C , response functions

$$C_h^\ell = \frac{1}{N} \mathbf{h}^\ell(\mathbf{x}, t) \cdot \mathbf{h}^\ell(\mathbf{x}', t') , \quad C_g^\ell(\mathbf{x}, \mathbf{x}', t, t') = \frac{1}{N} \mathbf{g}^\ell(\mathbf{x}, t) \cdot \mathbf{g}^\ell(\mathbf{x}', t') \quad (19)$$

$$R_{h\xi}^L(\mathbf{x}, \mathbf{x}', t, t') = -\frac{i}{N} \mathbf{h}^L(\mathbf{x}, t) \cdot \widehat{\boldsymbol{\xi}}^L(\mathbf{x}', t') \quad (20)$$

$$M_{\sigma\sigma C_\phi}^\ell = \frac{1}{E} \sum_k \sigma_k^\ell(\mathbf{x}, t) \sigma_k^\ell(\mathbf{x}', t') C_{\phi_k}^\ell(\mathbf{x}, \mathbf{x}', t, t') \quad (21)$$

$$M_{\sigma\sigma C_g}^\ell = \frac{1}{E} \sum_k \sum_k \sigma_k^\ell(\mathbf{x}, t) \sigma_k^\ell(\mathbf{x}', t') C_{g_k}^\ell(\mathbf{x}, \mathbf{x}', t, t') \quad (22)$$

$$M_{\sigma\sigma \mathcal{A}\mathcal{A}}^\ell = \frac{1}{E} \sum_k \sigma_k^\ell(\mathbf{x}, t) \sigma_k^\ell(\mathbf{x}', t') \mathcal{A}_k^\ell(\mathbf{x}, t) \mathcal{A}_k^\ell(\mathbf{x}', t') \quad (23)$$

$$\bar{R}_{\phi\xi}^\ell = -\frac{i}{E} \sum_k \sigma_k(\mathbf{x}, t) \left(\frac{1}{N_e} \phi(\mathbf{h}_k^{\ell,1}(\mathbf{x}, t)) \cdot \widehat{\boldsymbol{\xi}}_k^{\ell,1}(\mathbf{x}', t') \right) \quad (24)$$

$$\bar{R}_{g\chi}^\ell = -\frac{i}{E} \sum_k \sigma_k(\mathbf{x}, t) \left(\frac{1}{N_e} \mathbf{g}_k^{\ell,1}(\mathbf{x}, t) \cdot \widehat{\boldsymbol{\chi}}_k^{\ell,1}(\mathbf{x}', t') \right) \quad (25)$$

For each of these variables, there is a corresponding conjugate order parameter. Averaging over the initial random weights for each layer generates the following DMFT path integral over a set of order parameters \mathbf{Q}_{res}

$$Z = \int d\mathbf{Q}_{\text{res}} \exp(N\mathcal{S}(\mathbf{Q}_{\text{res}})) \quad (26)$$

resulting in the following $\mathcal{O}(1)$ action \mathcal{S} where we suppress data and time indices

$$\begin{aligned} \mathcal{S} = & \widehat{f} (f - \Phi^L \Delta - R_{h\xi}^L) - \widehat{R}_{h\xi}^L R_{h\xi}^L + \sum_\ell \left[C_h^\ell \widehat{C}_h^\ell + C_g^\ell \widehat{C}_g^\ell \right] \\ & + \nu \sum_\ell \left[\widehat{M}_{\sigma\sigma C_\phi}^\ell M_{\sigma\sigma C_\phi}^\ell + \widehat{M}_{\sigma\sigma C_g}^\ell M_{\sigma\sigma C_g}^\ell + \widehat{M}_{\dot{\sigma}\dot{\sigma} \mathcal{A}\mathcal{A}}^\ell M_{\dot{\sigma}\dot{\sigma} \mathcal{A}\mathcal{A}}^\ell - \widehat{R}_{\phi\xi}^\ell \bar{R}_{\phi\xi}^\ell - \widehat{R}_{g\chi}^\ell \bar{R}_{g\chi}^\ell \right] \\ & + \ln \mathcal{Z}_{\text{res}} + \nu \sum_{\ell=1}^L \ln \mathcal{Z}_{\text{exp}}^\ell \end{aligned} \quad (27)$$

where the residual stream single site measure is defined as

$$\begin{aligned} \mathcal{Z}_{\text{res}} = & \int \prod_\ell \mathcal{D}\bar{\chi}^\ell \mathcal{D}\widehat{\chi}^\ell \mathcal{D}\bar{\xi}^\ell \mathcal{D}\widehat{\xi}^\ell \mathcal{D}h^\ell \mathcal{D}\widehat{h}^\ell \mathcal{D}g^\ell \mathcal{D}\widehat{g}^\ell \exp \left(-\frac{\alpha_\star}{2} \sum_\ell \left[\widehat{\chi}^\ell \widehat{\chi}^\ell M_{\sigma\sigma C_\phi}^\ell + \widehat{\xi}^\ell \widehat{\xi}^\ell M_{\sigma\sigma C_g}^\ell \right] \right) \\ & \exp \left(-i \widehat{R}_{h\xi}^L h^L \xi^L + i \sum_\ell \widehat{\chi}^\ell [\bar{\chi}^\ell - \bar{R}_{\phi\xi}^\ell g^\ell] + i \sum_\ell \widehat{\xi}^\ell [\bar{\xi}^\ell - \bar{R}_{g\chi}^\ell h^\ell] \right) \\ & \exp \left(i \sum_\ell \widehat{h}^{\ell+1} [h^{\ell+1} - h^\ell - L^{-1} \bar{\chi}^\ell - \gamma_0 L^{-1} \Delta M_{\sigma\sigma C_\phi}^\ell g^{\ell+1}] \right) \\ & \exp \left(i \sum_\ell \widehat{g}^\ell [g^\ell - g^{\ell+1} - L^{-1} \bar{\xi}^\ell - \gamma_0 L^{-1} \Delta (M_{\sigma\sigma C_g}^\ell + M_{\dot{\sigma}\dot{\sigma} \mathcal{A}\mathcal{A}}^\ell) h^\ell] \right) \end{aligned} \quad (28)$$

$$\alpha_\star = \frac{N}{N_e E} \quad (29)$$

Similarly, the expert moment generating functions $\mathcal{Z}_{\text{exp}}^\ell$ have the form

$$\begin{aligned} \mathcal{Z}_{\text{exp}}^\ell &= \int \mathcal{D}p^\ell \mathcal{D}\hat{p}^\ell \mathcal{D}\mathcal{A}^\ell \mathcal{D}\hat{\mathcal{A}}^\ell \mathcal{D}C_{\phi_k}^\ell \mathcal{D}\hat{C}_{\phi_k}^\ell \mathcal{D}C_{g_k}^\ell \mathcal{D}\hat{C}_{g_k}^\ell \mathcal{D}C_{h_k \xi_k}^\ell \mathcal{D}\hat{C}_{h_k \xi_k}^\ell \\ &\quad \exp\left(-\hat{M}_{\sigma\sigma C_\phi}^\ell \sigma^\ell \sigma^\ell C_{\phi_k}^\ell - \hat{M}_{\sigma\sigma C_g}^\ell \sigma^\ell \sigma^\ell C_{g_k}^\ell - \hat{M}_{\dot{\sigma}\dot{\sigma} \mathcal{A}\mathcal{A}}^\ell \dot{\sigma}^\ell \dot{\sigma}^\ell \mathcal{A}^\ell \mathcal{A}^\ell\right) \\ &\quad \exp\left(i\hat{p}_k^\ell [p_k^\ell - \gamma_0 \Delta \dot{\sigma}_k^\ell \mathcal{A}_k^\ell C_h^\ell] + i\hat{\mathcal{A}}_k^\ell [\mathcal{A}_k^\ell - C_{h_k \xi_k}^\ell - \gamma_0 \Delta \sigma_k^\ell C_g^{\ell+1} C_{\phi_k}^\ell]\right) \\ &\quad \exp\left(C_{\phi_k} \hat{C}_{\phi_k} + C_{g_k} \hat{C}_{g_k} + C_{h_k \xi_k} \hat{C}_{h_k \xi_k} + N_e \ln \mathcal{Z}_{\text{within-exp}}^\ell\right) \end{aligned} \quad (30)$$

The within-expert distribution is defined as

$$\begin{aligned} \mathcal{Z}_{\text{within-exp}}^\ell &= \int \mathcal{D}\chi_k^\ell \mathcal{D}\hat{\chi}_k^\ell \mathcal{D}\xi_k^\ell \mathcal{D}\hat{\xi}_k^\ell \mathcal{D}\hat{h}_k^\ell \mathcal{D}h_k^\ell \mathcal{D}\hat{g}_k^\ell \mathcal{D}g_k^\ell \exp\left(-\frac{1}{2} [\hat{\chi}_k^\ell \hat{\chi}_k^\ell C_h^\ell + \hat{\xi}_k^\ell \hat{\xi}_k^\ell C_g^{\ell+1}] + i\hat{\chi}_k^\ell \chi_k^\ell + i\hat{\xi}_k^\ell \xi_k^\ell\right) \\ &\quad \exp\left(i\hat{h}_k^\ell (h_k^\ell - \chi_k^\ell - \gamma_0 \Delta \sigma_k C_h^\ell g_k^\ell) + i\hat{g}_k^\ell (\dot{\phi}(h_k^\ell) [\xi_k^\ell + \gamma_0 \Delta \sigma_k^\ell C_g^{\ell+1} \phi(h_k^\ell)])\right) \\ &\quad \exp\left(-\frac{1}{N_e} \hat{C}_{\phi_k}^\ell \phi(h_k^\ell) \phi(h_k^\ell) - \frac{1}{N_e} \hat{C}_{g_k}^\ell g_k^\ell g_k^\ell - \frac{1}{N_e} \hat{C}_{\phi_k \xi_k}^\ell \phi(h_k^\ell) \xi_k^\ell\right) \\ &\quad \exp\left(-\frac{i}{N_e} \hat{R}_{\phi \xi}^\ell \sigma_k^\ell \phi(h_k^\ell) \hat{\xi}_k^\ell - \frac{i}{N_e} \hat{R}_{g \chi}^\ell \sigma_k^\ell g_k^\ell \hat{\chi}_k^\ell\right) \end{aligned} \quad (31)$$

We let $N_e(N)$ and $E(N)$ be diverging functions for the hidden width and expert size as a function of residual stream width N at any fixed value of depth L . We assume the following condition to be satisfied

$$\lim_{N \rightarrow \infty} \frac{N}{N_e(N)E(N)} = \alpha_\star L < \infty \quad (32)$$

This is satisfied for many common scaling strategies. For instance, if FFN ratio N_e/N is fixed and E also diverges (at any rate) then this condition is satisfied as $\alpha_\star = 0$. Similarly, if E/N is fixed and N_e diverges (at any rate) then $\alpha_\star = 0$.

Large Expert Size For any diverging expert size $N_e \rightarrow \infty$ we can expand $\mathcal{Z}_{\text{within-exp}}^\ell$ to obtain a reduced action

$$\begin{aligned} N_e \ln \mathcal{Z}_{\text{within-exp}}^\ell &\sim -\hat{C}_{\phi_k}^\ell \{\phi(h_k^\ell) \phi(h_k^\ell)\} - \hat{C}_{g_k}^\ell \{g_k^\ell g_k^\ell\} - \hat{C}_{\phi \xi}^\ell \{\phi(h_k^\ell) \xi_k^\ell\} \\ &\quad - i\hat{R}_{\phi \xi}^\ell \sigma_k^\ell \{\phi(h_k^\ell) \hat{\xi}_k^\ell\} - i\hat{R}_{g \chi}^\ell \sigma_k^\ell \{g_k^\ell \hat{\chi}_k^\ell\} + \mathcal{O}(N_e^{-1}) \end{aligned} \quad (33)$$

where $\{\}$ represents an average over the following stochastic process defined by (which is a function of all of the per-expert order parameters) and has the structure

$$\begin{aligned} h_k^\ell &= \chi_k^\ell + \gamma_0 \Delta \sigma_k^\ell C_h^\ell g_k^\ell, \quad \chi_k^\ell \sim \mathcal{GP}(0, C_h^\ell) \\ g_k^\ell &= \dot{\phi}(h_k^\ell) [\xi_k^\ell + \gamma_0 \Delta \sigma_k^\ell C_g^{\ell+1} \phi(h_k^\ell)], \quad \xi_k^\ell \sim \mathcal{GP}(0, C_g^{\ell+1}) \end{aligned} \quad (34)$$

These equations provide the within-neuron distribution and dynamics as $N_e \rightarrow \infty$. We note that the response functions from the residual stream have no influence on these dynamics in this limit.

Large Residual Stream + Large Number of Experts The remaining order parameters Q_{res} are computed from a saddle point of \mathcal{S} . We let $\langle \rangle$ represent an average over the neuron measure defined by \mathcal{Z}_{res} and let $\langle \rangle$ represent an average over the

expert measure defined by \mathcal{Z}_{exp} and lastly let $\{\cdot\}$ represent an average over the within-expert neuron distribution

$$\frac{\partial \mathcal{S}}{\partial \widehat{C}_h^\ell} = C_h^\ell - \langle h^\ell h^\ell \rangle = 0 \quad (35)$$

$$\frac{\partial \mathcal{S}}{\partial \widehat{C}_g^\ell} = C_g^\ell - \langle g^\ell g^\ell \rangle = 0 \quad (36)$$

$$\frac{\partial \mathcal{S}}{\partial \widehat{M}_{\sigma\sigma C_{\phi_k}}^\ell} = M_{\sigma\sigma C_{\phi_k}}^\ell - [\sigma^\ell \sigma^\ell \{\phi(h_k^\ell) \phi(h_k^\ell)\}] = 0 \quad (37)$$

$$\frac{\partial \mathcal{S}}{\partial \widehat{M}_{\sigma\sigma C_{g_k}}^\ell} = M_{\sigma\sigma C_{g_k}}^\ell - [\sigma^\ell \sigma^\ell \{g_k^\ell g_k^\ell\}] = 0 \quad (38)$$

$$\frac{\partial \mathcal{S}}{\partial \widehat{M}_{\dot{\sigma}\dot{\sigma} \mathcal{A}\mathcal{A}}^\ell} = M_{\dot{\sigma}\dot{\sigma} \mathcal{A}\mathcal{A}}^\ell - [\dot{\sigma}^\ell \dot{\sigma}^\ell \mathcal{A}^\ell \mathcal{A}^\ell] = 0 \quad (39)$$

$$\frac{\partial \mathcal{S}}{\partial \widehat{R}_{\phi\xi}^\ell} = -\bar{R}_{\phi\xi}^\ell - i \left[\sigma^\ell \left\{ \phi(h_k^\ell) \widehat{\xi}_k^\ell \right\} \right] = 0 \quad (40)$$

$$\frac{\partial \mathcal{S}}{\partial \widehat{R}_{g\chi}^\ell} = -\bar{R}_{g\chi}^\ell - i \left[\sigma^\ell \left\{ g_k^\ell \widehat{\chi}_k^\ell \right\} \right] = 0 \quad (41)$$

$$\frac{\partial \mathcal{S}}{\partial \bar{R}_{\phi\xi}^\ell} = -\bar{R}_{\phi\xi}^\ell - i \left\langle \widehat{\chi}^\ell g^\ell \right\rangle = 0 \quad (42)$$

$$\frac{\partial \mathcal{S}}{\partial \bar{R}_{g\chi}^\ell} = -\bar{R}_{g\chi}^\ell - i \left\langle \widehat{\xi}^\ell h^\ell \right\rangle = 0 \quad (43)$$

The remaining saddle point equations give $\widehat{C} = 0$ and $\widehat{M} = 0$. The response functions can be rearranged as derivatives through integration by parts (Crisanti & Sompolinsky, 2018; Mignacco et al., 2020; Bordelon & Pehlevan, 2022; 2026)

$$-i\{\phi(h_k^\ell) \widehat{\xi}_k^\ell\} = \left\{ \frac{\partial \phi(h_k^\ell)}{\partial \xi_k^\ell} \right\}, \quad -i\{g_k^\ell \widehat{\chi}_k^\ell\} = \left\{ \frac{\partial g_k^\ell}{\partial \chi_k^\ell} \right\}. \quad (44)$$

Top-K Operation The top-K gating operation for $\kappa = K/E$ is well defined as a quantile thresholding operation under the mean-field measure over experts (averages represented by $[\cdot]$). Introduce the random variable $q = \sigma(p) + b$ and let $q_*(\kappa)$ represent the solution to the equation

$$[1_{q \geq q_*(\kappa)}] = \kappa \quad (45)$$

The variable $q_*(\kappa)$ is thus the lower end point of integration for the gating preactivation distribution that captures the top κ probability mass. The hard-routing gate variables which occur in the top-K routing are thus

$$\sigma^\ell(\mathbf{x}, t) = 1_{q \geq q_*(\kappa)} \sigma(p^\ell(\mathbf{x}, t)) \quad (46)$$

These are the hard gating variables which govern the evolution equations.

Final DMFT Equations The DMFT single site equations are the following. For the residual stream (reminder that $\alpha_* = \lim_{N \rightarrow \infty} \frac{N}{N_e(N)E(N)}$ is bounded).

$$\begin{aligned} h^{\ell+1}(\mathbf{x}, t) &= h^\ell(\mathbf{x}, t) + L^{-1} u^\ell(\mathbf{x}, t) \\ &+ L^{-1} \int dt' d\mathbf{x}' \left[\bar{R}_{\phi\xi}^\ell(\mathbf{x}, \mathbf{x}', t, t') + \gamma_0 p(\mathbf{x}') \Delta(\mathbf{x}', t') M_{\sigma\sigma C_{\phi_k}}^\ell(\mathbf{x}, \mathbf{x}', t, t') \right] g^{\ell+1}(\mathbf{x}', t') \\ g^\ell(\mathbf{x}, t) &= g^{\ell+1}(\mathbf{x}, t) + L^{-1} r^\ell(\mathbf{x}, t) \\ &+ L^{-1} \int dt' d\mathbf{x}' \left[\bar{R}_{g\chi}^\ell(\mathbf{x}, \mathbf{x}', t, t') + \gamma_0 p(\mathbf{x}') \Delta(\mathbf{x}', t') M_{\sigma\sigma C_{g_k}}^\ell(\mathbf{x}, \mathbf{x}', t, t') \right] h^\ell(\mathbf{x}', t') \\ u^\ell(\mathbf{x}, t) &\sim \mathcal{GP} \left(0, \alpha_* M_{\sigma\sigma C_{\phi_k}}^\ell(\mathbf{x}, \mathbf{x}', t, t') \right), \quad r^\ell(\mathbf{x}, t) \sim \mathcal{GP} \left(0, \alpha_* M_{\sigma\sigma C_{g_k}}^\ell(\mathbf{x}, \mathbf{x}', t, t') \right) \end{aligned} \quad (47)$$

All averages $\langle \rangle$ computed from the residual stream are averages over the above stochastic processes.

Next, for the expert distribution, we have

$$\begin{aligned} p_k^\ell(\mathbf{x}, t) &= \gamma_0 \int dt' \mathcal{A}_k^\ell(\mathbf{x}', t') \dot{\sigma}_k^\ell(\mathbf{x}', t') H^\ell(\mathbf{x}, \mathbf{x}', t, t') \\ b_k(t) &= b_k(0) + \gamma_0 \int dt' (\kappa - \mathbb{E}_{\mathbf{x}} 1_{q^\ell(\mathbf{x}, t) \geq q_*^\ell(\mathbf{x}, t)}) \\ \mathcal{A}_k^\ell(\mathbf{x}, t) &= C_{\phi_k \xi_k}^\ell(\mathbf{x}, \mathbf{x}, t, t) + \gamma_0 \mathbb{E}_{\mathbf{x}'} \int dt' \sigma_k^\ell(\mathbf{x}', t') C_g^{\ell+1}(\mathbf{x}, \mathbf{x}', t, t') C_{\phi_k}^\ell(\mathbf{x}, \mathbf{x}', t, t') \\ \sigma_k^\ell(\mathbf{x}, t) &= 1_{q^\ell(\mathbf{x}, t) \geq q_*^\ell(\mathbf{x}, t)} \sigma(p_k^\ell(\mathbf{x}, t)) \end{aligned} \quad (48)$$

These equations define the averaging operation over experts $\langle \rangle$. The main source of disorder from the initial condition arises from the random initial biases $b_k(0)$ for the router. The dynamics of neurons within expert have the form

$$\begin{aligned} h_k^\ell(\mathbf{x}, t) &= \chi_k^\ell(\mathbf{x}, t) + \gamma_0 \mathbb{E}_{\mathbf{x}'} \int dt' \Delta(\mathbf{x}', t') \sigma_k^\ell(\mathbf{x}', t') C_h^\ell(\mathbf{x}, \mathbf{x}', t, t') g_k(\mathbf{x}', t') , \quad \chi_k^\ell(\mathbf{x}, t) \sim \mathcal{GP}(0, C_h^\ell) \\ z_k^\ell(\mathbf{x}, t) &= \xi_k^\ell(\mathbf{x}, t) + \gamma_0 \mathbb{E}_{\mathbf{x}'} \int dt' \Delta(\mathbf{x}', t') \sigma_k^\ell(\mathbf{x}', t') C_g^{\ell+1}(\mathbf{x}, \mathbf{x}', t, t') \phi(h_k(\mathbf{x}', t')) , \quad \xi_k^\ell(\mathbf{x}, t) \sim \mathcal{GP}(0, C_g^{\ell+1}) \\ g_k^\ell(\mathbf{x}, t) &= \dot{\phi}(h_k^\ell(\mathbf{x}, t)) z_k^\ell(\mathbf{x}, t) \end{aligned} \quad (49)$$

The average $\langle \rangle$ over neurons within each expert are determined by the above stochastic process.

Large Depth Limit The large depth limit simply introduces a differential equation in layer time $\tau = \ell/L \in [0, 1]$ (Bordelon et al., 2023; Dey et al., 2025). The order parameters become functions of this “depth-time” τ

$$\begin{aligned} C_h^\ell(\mathbf{x}, \mathbf{x}', t, t')|_{\ell=\lfloor \tau L \rfloor} &\rightarrow C_h(\tau, \mathbf{x}, \mathbf{x}', t, t') \\ C_g^\ell(\mathbf{x}, \mathbf{x}', t, t')|_{\ell=\lfloor \tau L \rfloor} &\rightarrow C_g(\tau, \mathbf{x}, \mathbf{x}', t, t') \\ M_{\sigma\sigma C_\phi}^\ell(\mathbf{x}, \mathbf{x}', t, t')|_{\ell=\lfloor \tau L \rfloor} &\rightarrow M_{\sigma\sigma C_\phi}(\tau, \mathbf{x}, \mathbf{x}', t, t') \\ M_{\sigma\sigma C_g}^\ell(\mathbf{x}, \mathbf{x}', t, t')|_{\ell=\lfloor \tau L \rfloor} &\rightarrow M_{\sigma\sigma C_g}(\tau, \mathbf{x}, \mathbf{x}', t, t') \\ M_{\dot{\sigma}\dot{\sigma} \mathcal{A} \mathcal{A}}^\ell(\mathbf{x}, \mathbf{x}', t, t')|_{\ell=\lfloor \tau L \rfloor} &\rightarrow M_{\dot{\sigma}\dot{\sigma} \mathcal{A} \mathcal{A}}(\tau, \mathbf{x}, \mathbf{x}', t, t') \\ \bar{R}_{\phi\xi}^\ell(\mathbf{x}, \mathbf{x}', t, t')|_{\ell=\lfloor \tau L \rfloor} &\rightarrow \bar{R}_{\phi\xi}(\tau, \mathbf{x}, \mathbf{x}', t, t') \\ \bar{R}_{g\chi}^\ell(\mathbf{x}, \mathbf{x}', t, t')|_{\ell=\lfloor \tau L \rfloor} &\rightarrow \bar{R}_{g\chi}(\tau, \mathbf{x}, \mathbf{x}', t, t') \end{aligned} \quad (50)$$

We further assume that N, L, N_e are all diverging functions of residual stream width N

$$\alpha_* \equiv \lim_{N \rightarrow \infty} \frac{N}{L(N) E(N) N_e(N)} \quad (51)$$

Similarly, we have an SDE description for the residual stream variables

$$\begin{aligned} dh(\tau, \mathbf{x}, t) &= \sqrt{\alpha_*} du(\tau, \mathbf{x}, t) + d\tau \int dt' d\mathbf{x}' \left[\bar{R}_{\phi\xi}^\ell(\mathbf{x}, \mathbf{x}', t, t') + \gamma_0 p(\mathbf{x}') \Delta(\mathbf{x}', t') M_{\sigma\sigma C_{\phi_k}}^\ell(\mathbf{x}, \mathbf{x}', t, t') \right] g(\tau, \mathbf{x}', t') \\ \langle du(\tau, \mathbf{x}, t) du(\tau', \mathbf{x}', t') \rangle &= d\tau d\tau' \delta(\tau - \tau') M_{\sigma\sigma C_\phi}(\tau, \mathbf{x}, \mathbf{x}', t, t') \end{aligned} \quad (52)$$

For $\alpha_* = 0$, the Brownian motion term disappears and the residual stream dynamics reduce to a neural ODE, consistent with CompleteP scaling (Dey et al., 2025; Chizat, 2025).

E.1. Verifying Convergence in Soft Routing Model

In Figure 18 we verify the convergence of the dynamics to the theoretical mean field limit. The model is trained on a multi-index model of degree 4 in $D = 20$ dimensions. We plot the loss dynamics and the empirical $p_k(t)$ measures which are consistent across $E, N, N_e \gg 1$.

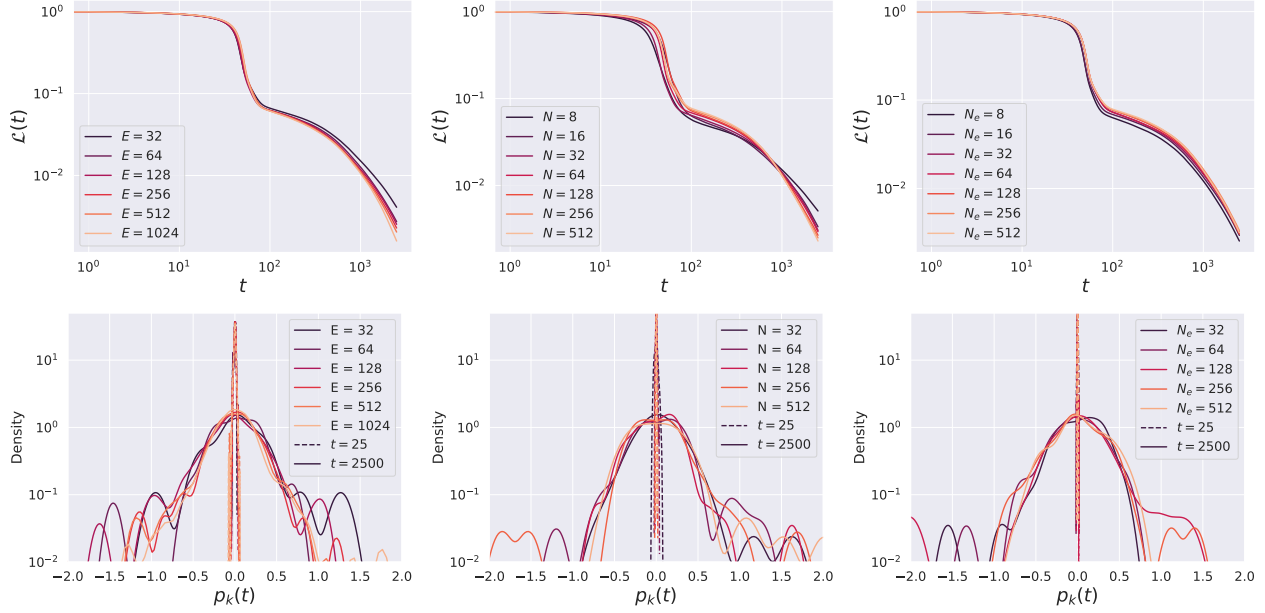


Figure 18. Loss dynamics $\mathcal{L}(t)$ and router preactivation $p_k(t)$ distribution (over experts) in a soft router MLP model trained on a multi-index polynomial target function. The parameterization achieves convergence to a well defined limiting dynamical system provided $\frac{N}{N_e E}$ is finite. From left to right: constant N and N_e (left), constant FFN ratio N_e/N with increasing N (middle), and constant N with increasing N_e .